Somatosensory & Motor Research 2003; 20(1): 45–69

Taylor & Francis
healthsciences

Time-dependence of SI RA neuron response to cutaneous flutter stimulation

B. L. WHITSEL[1,2], E. F. KELLY[3], M. QUIBRERA[1], M. TOMMERDAHL[2], Y. LI[2], O. V. FAVOROV[2,†], M. XU[2] and C. B. METZ[1]

[1]*Department of Cell and Molecular Physiology, University of North Carolina at Chapel Hill, Chapel Hill, NC 27599, USA;*
[2]*Department of Biomedical Engineering, University of North Carolina at Chapel Hill, Chapel Hill, NC 27599, USA;*
[3]*Department of Diagnostic Sciences, School of Dentistry, University of North Carolina at Chapel Hill, Chapel Hill, NC 27599, USA*

Abstract
Spike discharge activity of RA-type SI cortical neurons was recorded extracellularly in anesthetized monkeys and cats. Multiple applications (trials) of 10–50 Hz sinusoidal vertical skin displacement stimulation (''flutter'') were delivered to the receptive field (RF). Analysis revealed large and systematic temporal trends not only in SI RA neuron responsivity (measured as spikes/s and as spikes/stimulus cycle), but also in entrainment, and in phase angle of the entrained responses. In contrast to SI RA neurons, the response of RA skin afferents to comparable conditions of skin flutter stimulation exhibited little or no dynamics. The occurrence and form of the SI RA neuron response dynamics that accompany skin flutter stimulation are shown to depend on factors such as stimulus frequency and the locus of the recording site in the global cortical response pattern. Comparison of recordings obtained in near-radial vs tangential microelectrode penetrations further reveals that the SI RA neuron response dynamics that occur during skin flutter stimulation are relatively consistent *within*, but heterogeneous *across* column-sized regions. The observed SI RA neuron response dynamics are suggested to account, in part, for the improved capacity to discriminate stimulus frequency after an exposure (''adaptation'') to skin flutter stimulation (Goble and Hollins, *J Acoust Soc Am* **96:** 771–780, 1994). Parallels with recent proposals about the contributions to visual perception of short-term primary sensory cortical neuron dynamics and synchrony in multineuron spike activity patterns are identified and discussed.

Key words: *Somatosensation, cerebral cortex, vibrotaction, neural coding, response synchrony, information processing*

Introduction

Like the other primary sensory cortical areas, SI cortex traditionally has been viewed as a relatively passive analyzer of afferent drive delivered over ''hard-wired'' neuroanatomical connections. On this view, mechanisms active only or primarily during maturation select and stabilize these connections, and in this manner establish functional properties of sensory cortical neurons that in adults are essentially static.

That this view of SI cortex required modification was first established by M. M. Merzenich and colleagues, who demonstrated that in adult animals prolonged and substantial modifications of the normal pattern of cutaneous afferent drive—as achieved, for example, by digit amputation (Merzenich *et al.*, 1984) or extended exposure to the same pattern of vibrotactile stimulation (Recanzone *et al.*, 1992a,b)—are accompanied by modification of SI topographical organization, and by modifications of SI neuron receptive field (RF) and response properties. Although the central nervous system (CNS) site(s) and nature of the use-dependent mechanisms which underlie these modifications remain poorly understood, the observations that the cortical changes triggered by such manipulations of afferent drive are progressive, and require extended periods (hours to months) to attain full expression have been interpreted to indicate that they are mediated, at least in part, by irreversible or difficult-to-reverse Hebb-type alterations of CNS synaptic connectivity (Buonomano and Merzenich, 1998).

A rapidly expanding body of research indicates that neurons in primary sensory cortex also exhibit a very different type of functional plasticity. For example, visual cortical pyramidal neurons exhibit prominent, fully reversible, use-dependent modifications of both RFs and response properties that develop within tens of milliseconds of stimulus onset, and disappear within seconds of stimulus termination (Dinse *et al.*, 1990; Pettet and Gilbert, 1992; Shevelev *et al.*, 1992, 1998; Celebrini *et al.*, 1993; Das and Gilbert, 1995; DeAngelis *et al.*, 1995; Ringach *et al.*, 1997; Sugase *et al.*, 1999; Pack and Born, 2001; Pack *et al.*, 2001; Bredfeldt and

Correspondence: B. L. Whitsel, PhD, 155 Medical Science Research Bldg, Department of Cell and Molecular Physiology, CB# 7545, University of North Carolina, School of Medicine, Chapel Hill, NC 27599-7455, USA. Tel.: +1-919-966-1291; Fax: +1-919-966-6927; E-mail: bwhitsel@med.unc.edu
[†]Present address: School of Electrical Engineering and Computer Science, University of Central Florida at Orlando, Orlando, FL 32816-2362, USA.

ISSN 0899-0220 (print)/ISSN 1369-1651 (online)/03/010045-26 © 2003 Taylor & Francis Ltd
DOI: 10.1080/0899022031000083834

Ringach, 2002; for review see Kohn and Whitsel, 2002).

Given the many architectural and connectional features common to all primary sensory regions in cerebral cortex, it would be surprising if neurons in somatosensory cortex did not exhibit short-term response dynamics comparable to those described for visual cortical neurons. To date, few neurophysiological studies have addressed this possibility explicitly. Exceptional in this regard, however, are observations obtained in a study that examined the time-dependence of the response of SI pyramidal neurons (macaque monkey; areas 3b and 1) to a repetitive tactile motion (''skin brushing'') stimulus (Lee and Whitsel, 1992). When the interval between successive stimulus repetitions was less than 5 s, a substantial fraction (> 60%) of SI neurons displayed prominent and reproducible time trends in mean firing rate. Furthermore, it was typical for such a temporal trend in mean firing rate to be accompanied by a modification of RF size and/or sensitivity to the direction of tactile stimulus motion. A follow-up evoked potential mapping study (Lee *et al.*, 1992) demonstrated that the spatially distributed response of the rat sensorimotor cortical slice to electrical stimulation of axons in the underlying white matter modifies progressively during repetitive (5 Hz) input drive. Lee *et al.* (1992) interpreted their *in vitro* findings to indicate that mechanisms *intrinsic* to SI cortex were sufficient to account for the temporal trends in SI pyramidal neuron responsivity that occur in intact subjects during an exposure to repetitive skin brushing stimulation. Recent investigations of rat barrelfield cortex also have reported prominent, rapidly developing and fully reversible pyramidal neuron response dynamics, evoked in this case by repetitive movements of the mystacial vibrissae (Ghazanfar and Nicolelis, 1999, 2001; Ghazanfar *et al.*, 2000).

While vibrotactile stimuli have been used extensively to study the functional properties of SI neurons, the literature contains virtually no information about short-term dynamics in the SI neuron spike train responses to such stimulation. Insofar as the authors are aware only one previous study has examined this possibility explicitly, and that study reported finding little evidence of response dynamics associated with vibrotactile stimulation (Mountcastle *et al.*, 1969, p. 457). In contrast, optical intrinsic signal (OIS) imaging studies have reported that although the global pattern of SI activation produced by cutaneous flutter stimulation is initially diffuse and widespread, it contracts dramatically and rapidly with continuing stimulation—over a period of continuous flutter stimulation as brief as 3–10 s the size of the responding SI territory shrinks progressively and approaches the spatially discrete zone (in areas 3b and 1) that RF mapping observations indicate receives its dominant input from the stimulated skin site (Tommerdahl *et al.*, 1999a,b).

No previous study has sought parallels between the prominent time-dependence of the SI optical response to cutaneous flutter stimulation (Tommerdahl *et al.*, 1999a,b) and the spike train responses of individual SI neurons. The results presented in this paper fill this gap by providing evidence of substantial short-term temporal dynamics not only in the spike discharge activity a cutaneous flutter stimulus evokes from SI RA neurons, but also in the synchrony of the entrained oscillatory response of localized SI RA multineuron populations. In addition, the effects of multiple factors (stimulus frequency, amplitude, and position in the global response pattern) on the dynamics of the SI RA neuron response to flutter stimulation of the RF were systematically investigated.

Methods

Subjects/general procedures

All methods and procedures are consistent with USPHS policies and guidelines on animal care and welfare in biomedical research. They were reviewed and approved by an institutional committee prior to initiation of the experiments.

Following induction of anesthesia with 4% halothane in a 50/50 mix of nitrous oxide (N_2O) and oxygen, the trachea was intubated. A veterinary anesthesia machine (Forreger Compac-75) provided an anesthetic gas mix whose composition could be adjusted (typically 1.5–3.0% halothane in 50/50 N_2O/oxygen) to maintain a stable level of surgical anesthesia. Methylprednisolone sodium succinate (20 mg/kg) and gentamicin sulfate (2.5 mg/kg) were injected intramuscularly to lessen the probability of halothane-induced cerebral edema and prevent bacterial septicemia, respectively. Placement of a valved catheter into a superficial hindlimb vein enabled administration of 5% glucose, 0.9% NaCl, and drugs.

A 1.5 cm opening was trephined in the skull overlying SI cortex. A recording chamber (25 mm i.d.) was placed over the opening and cemented to the skull with dental acrylic. Wound margins were infiltrated with local anesthetic, closed with sutures and bandaged, and the dura overlying SI was resected. After the completion of all surgical procedures subjects were immobilized with norcuron (loading dose 0.25–0.5 mg/kg, i.v.; maintenance dose 0.025–0.05 mg/kg/h). From this point on, the animal was ventilated with a 50/50 mix of N_2O and oxygen and the concentration of halothane was adjusted (typically between 0.5 and 1.0%) to maintain heart rate, blood pressure, and the EEG at values consistent with general anesthesia. Rate and depth of ventilation were adjusted to maintain end-tidal CO_2 between 3.0 and 4.5%. Under these experimental/anesthetic conditions both SI neuron spontaneous and stimulus-evoked spike discharge activity patterns are highly reproducible over even prolonged (>1 h) time periods.

After obtaining a photograph of the exposed cortical surface the recording chamber was filled with artificial cerebrospinal fluid, and hydraulically sealed using a clear glass plate containing an ''o''-ring. The ''o''-ring permitted a microelectrode to be introduced into the chamber, inserted at the desired location within SI cortex, and advanced/retracted with a microdrive without opening the chamber. Maintenance of ''closed-chamber'' conditions minimizes the cortical and vascular movements associated with the cardiac and respiratory cycles and thus ensures stable, long-term extracellular recording of single neuron action potentials. The glass plate used to cap the recording chamber enabled visual determination (using an operation macroscope) of the precise locus and micrometer position at which each microelectrode penetration made initial contact with SI cortex.

Extracellular microelectrode recordings of SI RA neuron spike discharge activity were obtained sufficient in duration (≥ 20 min) to allow quantitative characterization of the time-dependency of the spike train response to cutaneous flutter stimulation. Neurons were classified as rapidly adapting (RA) if spike discharge activity (1) was evoked by application of gentle mechanical stimuli to only

a well-defined, localized skin region, and (2) occurred transiently in response to maintained mechanical contact with the RF. Such recordings were obtained in 11 monkeys (5 macaques—*Macaca nemistrina*, 6 squirrel monkeys—*Saimiri sciureus*), and 6 cats (*Felis domestica*). Electrolytically sharpened and glass-insulated tungsten wires with fine tips (impedance $3–5\times10^5\ \Omega$ at 10 kHz) were used. At the maximal depth of each penetration, and at other locations along the track where recordings of particular interest had been obtained, a microlesion was created by passing 1–10 μA of DC current through the microelectrode.

Euthanasia was accomplished by i.v. administration of pentobarbital (50 mg/kg), and intracardial perfusion with 0.9% saline followed by 10% formalin. The region of SI studied with microelectrode recordings was removed and serially sectioned at 30 μm. Monkey SI was sectioned in the sagittal plane, cat SI in the coronal plane. Sections were mounted on glass slides, Nissl-stained, coverslipped, and inspected microscopically. Areas 3a, 3b, 1 and 2 were distinguished on the basis of established cytoarchitectonic criteria (monkey—Powell and Mountcastle, 1959; Jones and Porter, 1980; Sur *et al.*, 1982; cat—Hassler and Muhs-Clement, 1964; McKenna *et al.*, 1981). High-resolution drawings of identified microelectrode tracks were prepared using a microscope with a drawing tube attachment. The sites at which SI RA neuron spike discharge activity was recorded were reconstructed using the three types of micrometer readings entered into the permanent experimental log during each microelectrode penetration: (1) position where the microelectrode made initial contact with the pial surface; (2) locus at which each record of spike discharge activity was obtained; and (3) depth at which each microlesion was placed.

In eight experiments (six squirrel monkeys, two cats) the OIS evoked in SI by cutaneous flutter stimuli was recorded prior to microelectrode recording. The imaging system consisted of a computer-interfaced CCD camera, the light source, guide and filters required for near-infrared (833 nm) illumination of the cortical surface, a focusing device, and a recording chamber capped by an optical window (for additional methodological details see Tommerdahl *et al.*, 1999a,b). Use of near-infrared illumination not only minimizes the contributions to OIS images of the changes in blood flow and flow/volume that normally accompany cortical neuronal activation, but at this wavelength the OIS exhibits substantially higher spatial and temporal resolution than at lower wavelengths (Malonek and Grinvald, 1996; Tommerdahl and Whitsel, 1996; Tommerdahl *et al.*, 1999a,b; Shtoyerman *et al.*, 2000; Shoham and Grinvald, 2001). Once OIS images of the global SI response to a flutter stimulus had been obtained, the optical recording system was disassembled and replaced with the apparatus for extracellular microelectrode recording. The goal of the microelectrode recording component of each experiment was to characterize the spike train responses of RA neurons to a preselected condition of skin flutter stimulation (the "standard mapping stimulus") at contrasting locations within the stimulus-evoked optical response pattern.

Recordings of flutter-evoked RA afferent spike discharge activity were obtained as the terminal phase of seven experiments (five monkeys, two cats). Afferents were classified as rapidly adapting (RA; more precisely as RA-I; Vallbo *et al.*, 1984) if (1) spontaneous spike discharge activity was absent or very low (<2 spikes/s), (2) RF size was small, and (3) the spike discharge activity evoked by skin stimulation met the criteria stated previously for SI RA neurons. All recordings from afferents were obtained under deep pentobarbital anesthesia (35–40 mg/kg initial dose; supplemented as needed) from fine filaments dissected from a peripheral nerve. The details of our methods of afferent recording were described in the two previous papers in this series (Whitsel *et al.*, 2000, 2001). The cortical neuron and afferent recordings were subjected to identical analyses in order to detect and measure time-dependencies in the response to cutaneous flutter (see below).

Vibrotactile stimulation

A servo-controlled mechanical stimulator (Chubbuck, 1966) was used to deliver constant-amplitude sinusoidal vertical skin displacement stimuli. The stimulator contacted the skin via the flat end of a plastic cylindrical probe (2 or 5 mm in diameter) threaded to the stimulator shaft. Sinusoidal probe motion began at phase zero (at 1.0 mm skin indentation), and initially advanced further into the skin. Since peak-to-peak amplitude of the sinusoid never was greater than 0.4 mm, the probe remained in contact with the skin during stimulation. In most studies the probe continued to indent the skin during the interval between successive stimuli ("trials"). In a few instances, the flutter stimuli were superimposed on an intermittent "pedestal"—i.e., in these studies the probe was maintained in a position above the skin surface prior to stimulation, advanced rapidly (10 ms) to produce 1.0 mm of skin indentation at 100–200 ms before the onset of sinusoidal stimulation, and retracted to the off-the-skin rest position 100–200 ms after stimulus termination. The specific conditions of flutter stimulation used to study each neuron/neuronal grouping/afferent will be described in the Results.

Neural data collection/analysis

Spike discharge activity and an analog signal of stimulus position were digitized at 20 kHz and stored as an electronic file. Software allowed post-experimental display and review of both neuroelectrical and stimulator events. A high-resolution monitor enabled inspection of the relationship between spike firing and stimulator events, evaluation of action potential waveforms, and discrimination (using voltage windows) of spikes attributable to different neurons or afferent fibers. For each recording 1–4 non-overlapping voltage windows were selected such that each window included action potentials attributable either to only a single, or a small grouping (usually 2–5) of neurons/afferents. The electronic file generated for every run contained the times of occurrence of the action potentials falling within each voltage window, and the times of specific stimulator events (onset and termination of the pedestal, onset of each individual stimulus cycle, termination of each trial, etc.).

Two aspects of spike discharge activity are especially relevant to the perception of vibrotactile stimuli, and these were measured and evaluated separately. The first, *responsivity* (spikes/cycle), was measured by counting the number of spikes in a designated time period and then dividing that count by the number of stimulus cycles. Incomplete stimulus cycles were ignored in this calculation. No correction was made for the significant amounts of spontaneous or background activity typically present, since adjusted and unadjusted responsivities to vibrotactile stimulation for RA afferents and SI RA neurons are highly correlated (*c.* 0.95, Whitsel *et al.*, 2001). To assess the time-dependency of responsivity, plots of spikes/cycle vs stimulus presentation number and/or time after stimulus onset were generated for each recording. Responsivity to skin flutter also was measured by computing the average rate of spike firing (mean spikes/s) over a time window larger than the stimulus cycle (e.g., over the full period of stimulation).

Entrainment, the organization of spike discharge activity into orderly temporal patterns coupled to the sinusoidal motion of the stimulus, was assessed using three measures which, collectively, enable entrainment to be measured quantitatively under a wide variety of stimulus conditions (Whitsel *et al.*, 2000, 2001). All three measures take values between 0.0 and 1.0, 1.0 indicating perfect entrainment. The first, $\mathbf{r}_1$, derives from the theory of circular statistics (Batschelet, 1981), and measures the tendency of spikes to cluster near a single modal or most-favored position in the stimulus cycle. This behavior corresponds to the classical view of neuronal entrainment as developed by Talbot *et al.* (1968) for skin mechanoreceptive afferents. The second, $\mathbf{r}_2$, extends the approach embodied by $\mathbf{r}_1$ to the specific and physiologically common situation in which spikes are generated at two modal positions approximately 180° apart in the stimulus cycle. This "bipolar" response pattern often occurs, for example, for Pacinian (PC, also termed RA-II) afferents even at low amplitudes of sinusoidal stimulation, and for RA afferents and SI cortical RA-type neurons exposed to moderate-to-large stimulus amplitudes (Johansson *et al.*, 1982; Whitsel *et al.*, 2000, 2001).

The third measure of entrainment was obtained by transforming the spike train record into a series of samples spaced equally in time, using an algorithm demonstrated to yield unbiased and alias-free estimates of the power spectrum (French and Holden, 1971a,b). This "resampling" of the spike train record was carried out at a rate greater than or equal to ten times the stimulus frequency, in order to capture a minimum of five harmonics in the power spectrum. The transformed record, in turn, was centered, detrended, converted to standard scores (mean zero, variance 1) in order to remove variation due to the overall response level, and the power spectrum calculated using conventional FFT-based methods (Marple, 1987). The resulting measure of neuronal entrainment, $\mathbf{r}_s$, reflects the proportion of signal amplitude that

corresponds to the stimulus frequency and its integral harmonics. Whitsel *et al.* (2000) demonstrated that $\mathbf{r}_s$ approximates $\mathbf{r}_1$ for monopolar patterns of phase-locked spike discharge activity, approximates $\mathbf{r}_2$ for bipolar patterns, and yields high values for many additional, more complex patterns that neither $\mathbf{r}_1$ nor $\mathbf{r}_2$ can effectively measure. In this paper we use the highest of the three measures for a particular record as the optimal measure of entrainment for that record—denoted "$\mathbf{r}_b$". To assess the time-dependency of entrainment, plots of $\mathbf{r}_b$ vs stimulus presentation number and/or $\mathbf{r}_b$ vs time after stimulus onset were generated for each record.

The circular statistics $\mathbf{r}_1$ and $\mathbf{r}_2$ are associated uniquely with an additional parameter, the mean phase angle of the response. This angle has no absolute meaning, since it depends on factors such as stimulus frequency and amplitude, as well as unknowns such as receptor utilization times, conduction distance, and conduction velocity. Under constant stimulus conditions, however, a systematic *change* in phase angle with increasing time after stimulus onset is indicative of dynamics in a neuron's response to stimulation. Therefore, for recordings which showed statistically significant entrainment of the $\mathbf{r}_1$ or $\mathbf{r}_2$ type we also generated plots of phase angle vs stimulus presentation number and/or phase angle vs time after stimulus onset. Statistical significance of each measured value of entrainment was assessed using the Rayleigh test of uniformity (Batschelet, 1981).

Systematic time-dependent changes in the distribution of SI RA neuron spike firing within the stimulus cycle also were studied by visual examination of cycle histograms constructed from activity recorded "early" (e.g., between 0 and 1 s after stimulus onset) vs "late" (e.g., between 4 and 5 s after stimulus onset) in the period of flutter stimulation. Such changes also were quantified by forming a "ratio plot" obtained by first computing the probability density of spike firing independently for both the late and early periods of stimulus-evoked activity, and then dividing the former by the latter. Probability densities were estimated from the spike timing data using the non-parametric method of Fisher (1993, pp. 24–30).

Quantitative treatment of the information obtained from the samples of neurons/afferents studied under the same conditions consisted of analyses of variance using the response measures as dependent variables, and descriptors of the stimulus parameters as the independent variables. Details of each such analysis are provided at the appropriate point in the text. Statistical analyses and plots were generated using SYSTAT, SAS, and MATLAB under Windows 2000.

Results

Evidence presented in the first paper of this series (Whitsel *et al.*, 2000) demonstrated that the spike train response of an RA afferent to flutter stimulation of the RF remains regular and stable even when the stimulus is applied continuously over a prolonged period (e.g., 15 s). In particular, RA afferent responsivity (spikes/cycle) declines only to a minor extent (10–20%) during prolonged exposure to either a continuous or an intermittent, rapidly repeated flutter stimulus, and entrainment remains consistently high (~ 0.9) and exhibits no temporal trends or dependence on any other measured factor. Similarly, the phase angle associated with the entrained response of an RA afferent is highly stable, apart from a small increase that typically occurs within the first 100–500 ms following stimulus onset (Whitsel *et al.*, 2000, Fig. 6–8 in that paper).

With this already published evidence of temporal stability of the response of RA afferents as background, consider the single SI RA neuron whose response to 25 Hz stimulation of the RF center is summarized in Fig. 1. This SI RA neuron's responsivity declined during stimulation to an extent substantially larger than the decline exhibited by most RA afferents studied under the same stimulus conditions—$\sim 50\%$ (left column, 2nd panel from top). In even more striking contrast to the behavior typical of RA afferents, both magnitude of entrainment and the phase angle of this SI RA neuron's entrained response increased progressively and substantially during stimulation, within and across trials (panels in the 3rd row from top).

The character of the time-dependent changes in the spike firing pattern of this same SI RA neuron is made apparent by overlaying the cycle histograms generated from the activity recorded during the initial (0–1 s) vs final (14–15 s) parts of the stimulus period (top right). The activity recorded during the initial second exhibits only a modest level of entrainment, and it is of the $\mathbf{r}_2$ (bipolar) type—i.e., there are two distinct modes of spike activity within the stimulus cycle, the second mode occurring approximately one half-cycle later than the first. After 14 s of continuous stimulation (see overlaid cycle histograms at top right), however, the second mode of spike firing is virtually absent. In addition to the obvious loss of activity during the second half of the stimulus cycle, the cycle histograms in Fig. 1 (top right) reveal that a lesser, but still considerable loss of responsivity also occurred in the leading half of the cycle. Interestingly, however, the responsivity loss in the leading half of the stimulus cycle differs from the loss in the trailing half-cycle—i.e., the loss of responsivity in the trailing half-cycle is "uniform" (distributed equally within this half-cycle), but in the leading half-cycle the loss is "selective" in that most of it occurs early in this half-cycle. As a result of these two very different time-dependent modifications of this RA neuron's spike firing pattern, during the last second (14th–15th s) of stimulation the spike activity associated with the flutter stimulus becomes "concentrated" within a narrow temporal window positioned relatively late (between 14 and 18 ms after stimulus onset) in the initial half-cycle of the stimulus period.

Figure 2 shows that the same SI RA neuron exhibited very similar time-dependent changes in a subsequent run in which the conditions of flutter stimulation were the same, *except stimulus duration*, which was substantially shorter than in the previous run (3 vs 15 s). The run that yielded the data in Fig. 2 was carried out 20 min after the run that provided the data in Fig. 1. The results in Fig. 2 demonstrate that, similar to the results obtained with the 15 s stimulus, 3 s of continuous skin flutter stimulation of the RF center led to prominent time-dependent modifications of this neuron's (i) responsivity (as with the 15 s stimulus, the loss of responsivity was distributed non-uniformly—i.e., the loss occurred at most locations within the trailing half-cycle, but virtually exclusively at early points in the leading half-cycle), (ii) entrainment (increase), and (iii) phase angle (increase).

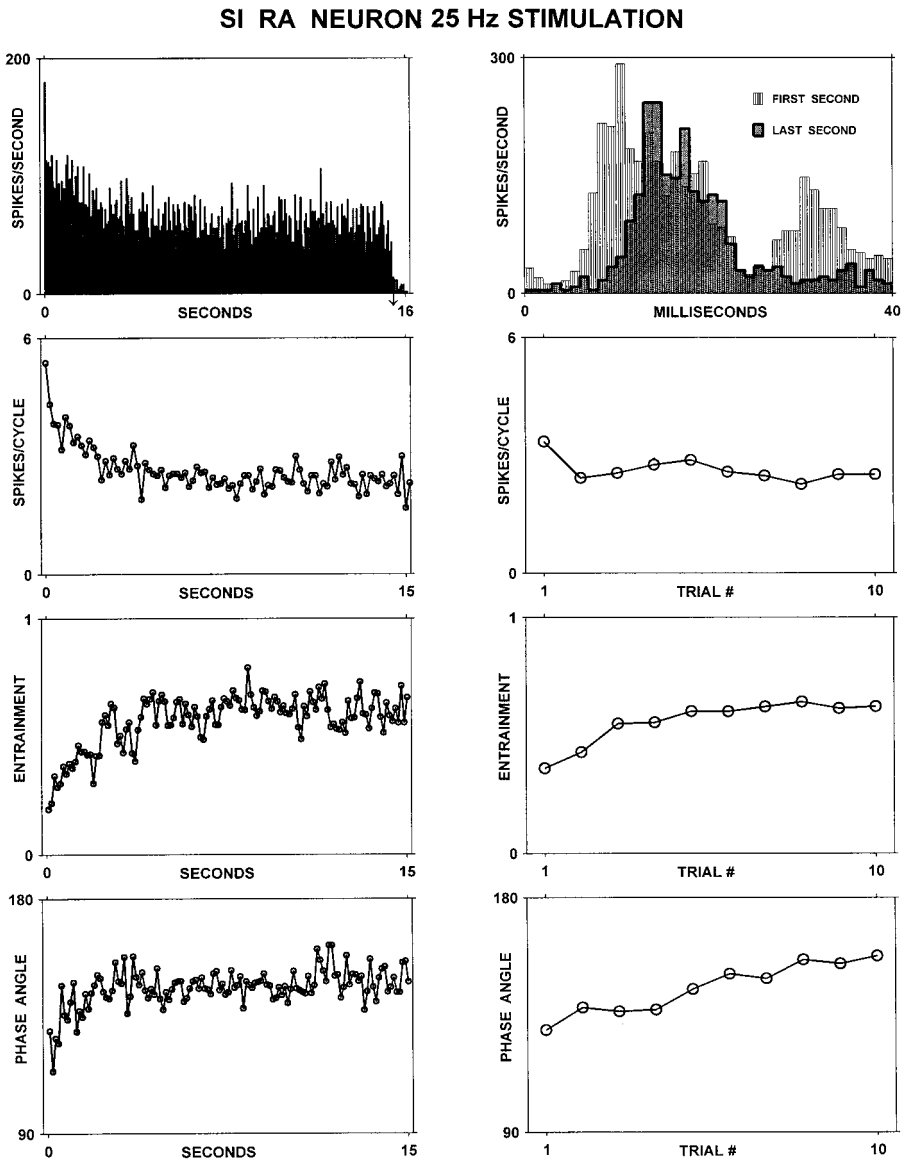

FIGURE 1. Response dynamics associated with 25 Hz stimulation of the RF center of an area 1 neuron (layer IV). RF on volar tip of digit 3 (macaque monkey). Stimulus duration 15 s; amplitude 200 μm; ISI 3 s; stimulator probe 5 mm diameter; ten trials. Panels on left: PST (bin width 50 ms—at top); spikes/stimulus cycle vs time (2nd from top); entrainment vs time (3rd from top); phase angle vs time (bottom). Each datapoint in plots on left indicates average (over ten trials) of the activity in six successive stimulus cycles. Top panel on right: Superimposed cycle histograms (bin width 1 ms) generated from activity recorded during initial (14th) and final (15th) seconds of stimulation; responsivity vs trial number (2nd from top); entrainment vs trial number (3rd from top); and phase angle vs trial number (bottom). Each datapoint in plots on right indicates average for that trial.

The data in Fig. 3 were obtained in a third run carried out on the same SI RA neuron whose data are illustrated in Figs. 1 and 2—the observations in Fig. 3 are of interest not only because they document the reproducibility of this neuron's response dynamics, but also because they provide a more complete picture of the temporal evolution of the pattern of spike firing during flutter stimulation of the RF center. As was evident in Figs. 1–2, Fig. 3 reveals that once again mean rate of spike firing declined progressively after stimulus onset (spike raster and PST plots in top and middle panels in center column), and progressive changes occurred in the temporal position of spike firing within the stimulus cycle. As in the previous runs (shown in Figs. 1 and 2), the cycle histograms generated for the activity recorded in successive 250 ms intervals during the first 1 s of stimulation (left column, Fig. 3) are of the $\mathbf{r}_2$-type (bipolar), with two peaks of spike firing within the stimulus cycle separated by approximately a half-cycle. However, after 1,500–2,750 ms of continuous stimulation (cycle histograms in panels on right) there was decreased spike firing at all points in the second half of the stimulus cycle, whereas spike firing had become more concentrated at points late in the first half of the stimulus cycle. These systematic time-dependent changes in the distribution of spike firing within the stimulus cycle are fully consistent with the plots of $\mathbf{r}_1$ and $\mathbf{r}_2$ vs time after onset of flutter stimulation (bottom panel, middle column).

The reproducible and highly orderly temporal evolution of the distribution of spike firing within the stimulus cycle exhibited by the exemplary SI RA

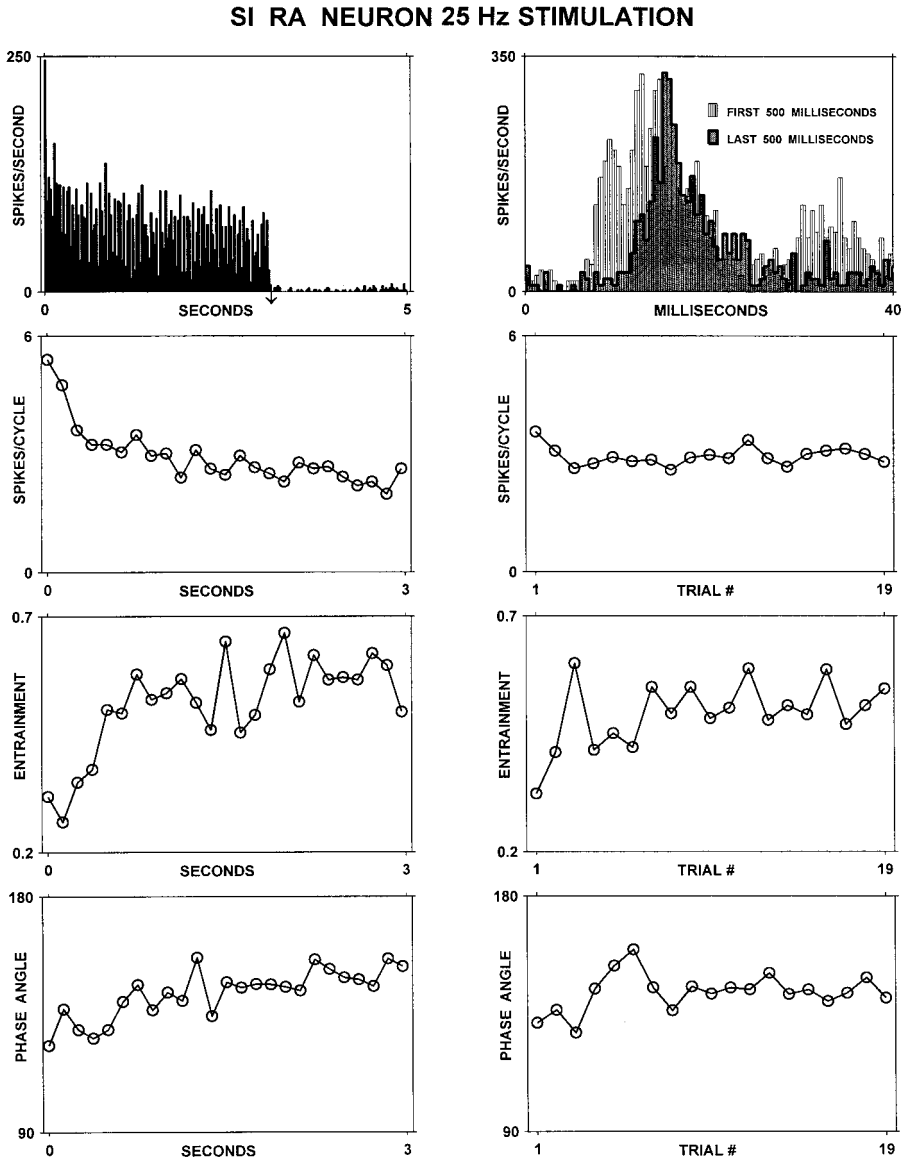

FIGURE 2. Same RA neuron as in Fig. 1. Stimulus conditions same as in Fig. 1, except duration was 3 s. Nineteen trials. Format same as Fig. 1. PST bin width 25 ms. Cycle histograms (bin width 0.5 ms) for activity recorded during the initial and final 500 ms of the stimulus period.

neuron in Figs. 1–3 contrasts sharply with the temporally stable spike firing behavior of RA afferents studied under similar stimulus conditions (Whitsel *et al.*, 2000). This contrast is illustrated in Fig. 4, which shows at high resolution the temporal history of spike firing for a representative RA afferent (top) and another SI RA neuron (bottom)—this afferent and neuron were studied using the same conditions of cutaneous flutter stimulation. Whereas the afferent's bipolar distribution of spike firing within the stimulus cycle exhibits great consistency over the full period of flutter stimulation (stimulus duration = 4 s), the distribution of spike firing within the stimulus cycle for the SI RA neuron studied using the same stimulus conditions is widespread initially (indicating relatively poor entrainment early in the response), but thereafter it progressively concentrates toward a position relatively late in the stimulus cycle. In other words, in striking contrast to the time-invariance of RA afferent entrainment and response phase angle, for the SI RA neuron whose data are shown at the bottom of Fig. 4 (as for the SI neuron in Figs. 1–3) both entrainment and phase angle varied systematically (both increased) with increasing time after onset of flutter stimulation.

The dynamic trends in the response of SI RA neurons during flutter stimulation of the RF not only are very similar from one run to the next (e.g., Figs. 1–3), but they also are reproducible from one stimulus to the next if sufficient time between successive stimulus applications is allowed. Figure 5 (bottom row, left and middle panels), for example, shows the consistency, across contiguous groups of just three trials (intertrial interval was 5 s), of the large within-trial increases in entrainment and phase angle exhibited by yet another SI RA neuron.

The main focus of this paper is on the SI RA neuron response dynamics observed using cutaneous

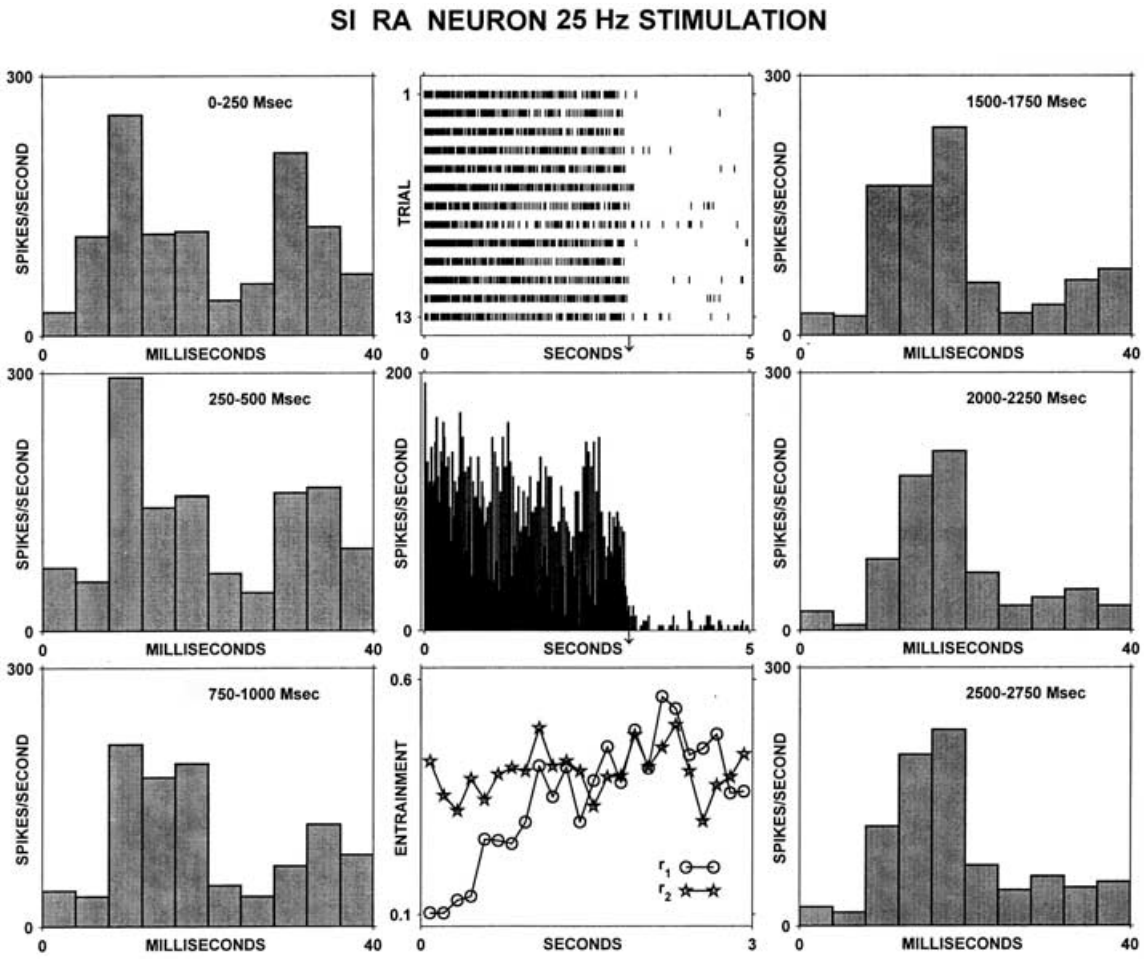

FIGURE 3. Same neuron as in Figs. 1 and 2. Stimulus conditions as in Fig. 2; results from a different run than the run that provided the observations in Figs. 1 and 2. Raster plot (middle column at top) shows spike train evoked by each of the 13 stimulus applications; PST is shown in middle column, 2nd from top (bin width 50 ms). Cycle histograms (columns on left and right; bin width 4 ms) showing that, as in the previous runs, the distribution of spike activity within the stimulus cycle again modified systematically with increasing time after stimulus onset. Plots—in bottom panel of middle column—comparison of the $\mathbf{r}_1$ and $\mathbf{r}_2$ measures of entrainment vs time after stimulus onset. Note that $\mathbf{r}_2$ yielded the higher estimates of entrainment during the initial 1–2 s of stimulation—at this time there was a prominent peak in spike discharge in both the first and second halves of the stimulus cycle (see cycle histograms).

flutter stimuli of duration 3–15 s, separated from one another by no-stimulus periods of at least equal length. However, large and reproducible across-trial RA neuron response dynamics also were observed when a brief-duration flutter stimulus was re-applied rapidly to the RF center. Figure 6, for example, summarizes the across-trial results obtained from a neuron that was studied in 17 different runs carried out over a period of approximately 3 h, each run consisting of 36–38 presentations (ISI 1 s) of a 0.8 s duration 10 Hz stimulus. The interval between successive runs was 3–15 min. For this neuron the main effect of such intermittent, but rapidly repeated and brief flutter stimulation of the RF center was a large, progressive, and reproducible across-trial increase in the phase angle of the response (bottom panels). This time-dependence of the phase angle of the entrained response was visually evident in the data obtained in all 17 of the runs, and it was independently significant ($p < 0.01$) for 15 of them. Furthermore, even though the RA neuron in Fig. 6 exhibited unusually high and stable entrainment (middle panels), the trial-by-trial variation in entrainment it did exhibit was strongly associated with the trial-by-trial variation in phase angle. Specifically, trial-by-trial phase angle and entrainment were strongly and positively correlated ($r = 0.70$, $p < 0.002$), and the correlation between mean entrainment and mean phase angle for each run was even stronger ($r = 0.86$; $p \ll 0.001$). Trial-by-trial entrainment and responsivity were negatively correlated ($r = -0.40$), but this was only marginally significant ($p < 0.07$).

In summary, the initial experiments of this study revealed large and reproducible time-dependent changes not only in SI RA neuron responsivity, but also in entrainment and phase angle during continuous 3–15 s or rapidly repeated, short-duration flutter stimulation of the RF center. Individually significant temporal trends in both entrainment and phase angle were detected in a substantial majority of both the 64 single SI RA neurons (73%) and the 94 small SI RA neuron groupings (64%) we studied, whereas none of the recordings obtained from 26 RA afferents exhibited such trends under comparable stimulus conditions. With stimulation of the RF

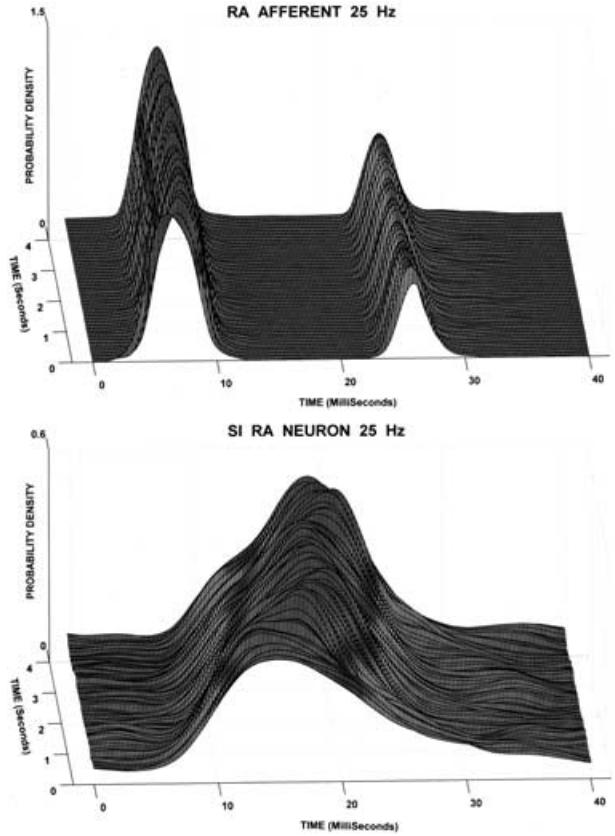

FIGURE 4. Probability density surfaces (PDSs) showing probability of spike firing within the stimulus cycle at different times after onset of flutter stimulation (every 100 ms for the afferent; every 50 ms for the SI RA neuron). Top: PDS generated from the data recorded from RA afferent. Bottom: PDS generated from data recorded from SI RA neuron (layer III, area 3b). This afferent and SI neuron were studied using the same conditions of stimulation—25 Hz, 200 μm peak-to-peak amplitude; 5 mm diameter contactor; ITI 5 s. The RF of the afferent was on the radial edge of digit 1 of the hand (macaque monkey); for the RA neuron the stimulus was applied to the RF center on the contralateral hypothenar eminence (squirrel monkey). Probability densities were estimated using nonparametric method (Fisher, 1993, pp. 24–30).

center at frequencies between 10 and 50 Hz, and at peak-to-peak amplitudes between 100 and 400 μm, SI RA neuron entrainment typically increased progressively (e.g., Figs. 1–5), although for a minority of neurons (~15%) it remained consistently high throughout the period of stimulation (e.g., Fig. 6).

In a very small minority (~10%) of the recordings carried out in our initial experiments flutter stimulation led to a large and highly significant decline (negative temporal trend) in both RA neuron entrainment and responsivity. Importantly, it was recognized early on that such declines in entrainment and in responsivity tended to occur when the stimulus conditions were non-optimal (e.g., when the flutter stimulus inadvertently was delivered to a skin site other than the RF center, or when a frequency of flutter stimulation was used that led to a rate of spike firing substantially less than that evoked by 25 Hz stimulation). Moreover, when such deviant response dynamics were observed, a modification of stimulus conditions (most frequently a minor adjustment of stimulator position) led to response dynamics similar to those exhibited by the great majority of RA neurons we studied using flutter stimulation of the RF center. Such qualitative observations led us to attempt, in a subsequent series of experiments, to more systematically evaluate the effects of selected factors on the SI RA neuron dynamics associated with skin flutter stimulation.

The observations in Fig. 7 suggest that *frequency* of flutter stimulation (of the RF center) exerts a considerable influence on both the magnitude and form of SI RA neuron response dynamics. For this RA neuron responsivity (spikes/s; see PSTs on left) during the initial 1 s of the response evoked by each frequency of stimulation was similar, and although responsivity declined progressively with continuing stimulation at all three stimulus frequencies, both the magnitude and rate of the decline in responsivity were greater at the higher (25 and 50 Hz) stimulus frequencies. Like responsivity, entrainment (top right) also remained relatively stable and at approximately the same value during the initial 1 s of the response to each frequency of stimulation (10, 25 and 50 Hz). However, at times greater than 1 s after the onset of flutter stimulation this RA neuron's entrainment improved progressively with continuing stimulation at both 10 and 25 Hz, whereas its entrainment deteriorated progressively when the frequency of stimulation was 50 Hz (entrainment vs time plot and circular histograms on the right).

Evidence showing that frequency of vibrotactile stimulation of the RF center systematically influences the form of SI RA neuron entrainment dynamics is summarized in Fig. 8. As a group, the 39 SI RA neurons studied to date exhibited a strong tendency for entrainment to increase during a 3 s exposure to RF center stimulation when the frequency of stimulation was located centrally (between 20 and 35 Hz) within the band of frequencies (6–50 Hz) humans experience as cutaneous flutter. The largest average increase in entrainment that occurred during stimulation of the RF center was at 29 Hz, and progressively lesser increases in entrainment occurred at higher or lower stimulus frequencies. Interestingly, at both extremes of the frequency range we studied (i.e., at 12 Hz and at frequencies $\geq$ 150 Hz) average across-neuron entrainment did not increase, but *declined* during stimulation of the RF center (this decrease was statistically significant only at 12 Hz; $p < 0.05$). In contrast, for the 24 RA afferents that we studied using the same stimulus conditions, entrainment (and responsivity; not shown in Fig. 8) exhibited only minor temporal dynamics, regardless of the frequency of vibrotactile stimulation.

We next studied the effects of *stimulus amplitude*. In these studies the flutter stimulus (25 Hz) was applied to the RF center of each of 37 SI RA neurons at five different amplitudes (10, 25, 50, 100 and 200 μm, peak-to-peak; stimulus duration was always 5 s). Amplitude of stimulation was incremented to

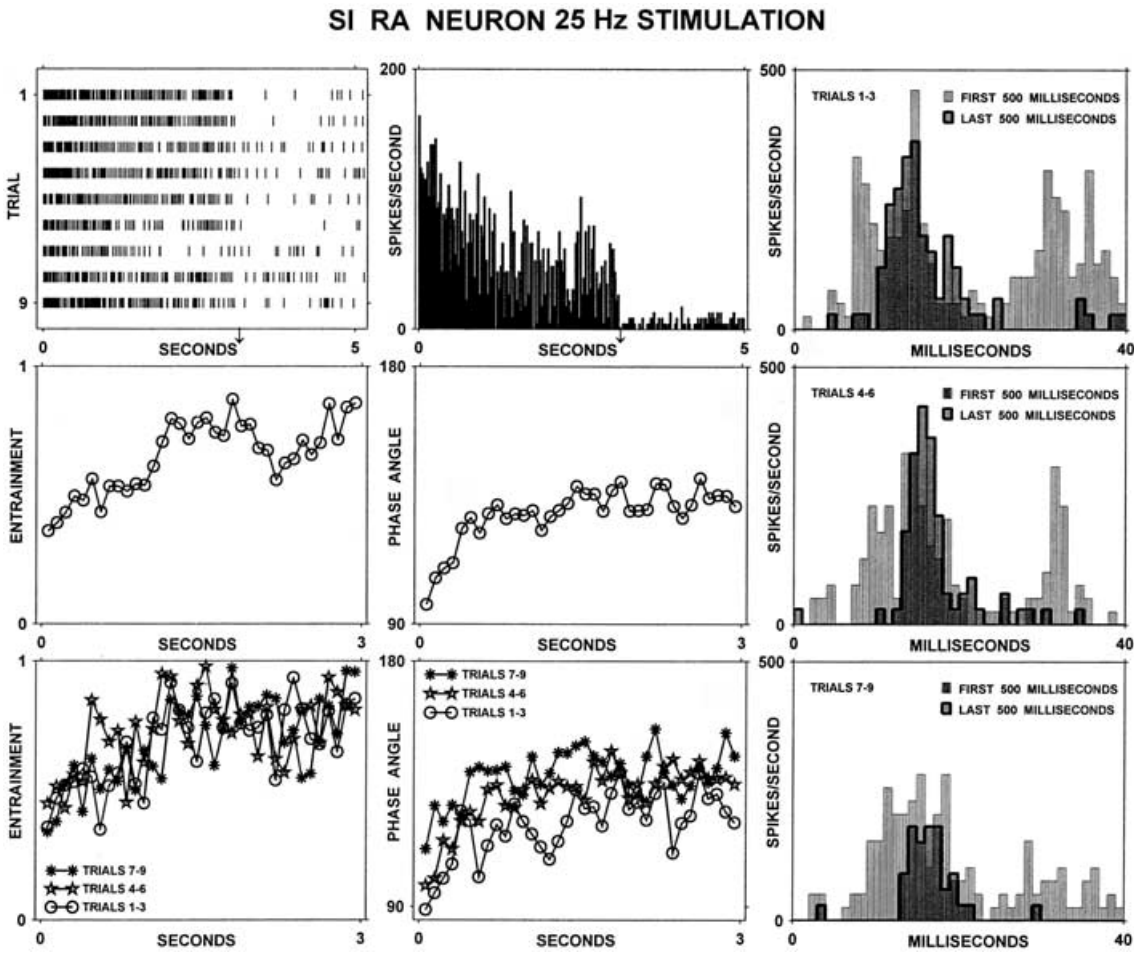

FIGURE 5. Reproducibility of within-trial SI RA neuron dynamics associated with skin flutter stimulation. Neuron in layer III of area 3b (macaque monkey). Upper left panel: Raster plot showing spike train responses to nine stimulus presentations (duration 3 s). Top center panel: PST, bin width 50 ms. Left column, 2nd panel from top: Plot of average entrainment vs time (across all nine trials). Middle column, 2nd panel from top: Plot of average phase angle vs time (across all nine trials). Left and middle columns, bottom panels: Three superimposed entrainment vs time plots (left), and three superimposed phase angle vs time plots (middle) constructed from spike train data recorded from the same neuron during stimulus trials 1–3 (circles), 4–6 (stars), and 7–9 (asterisks). Each datapoint indicates the average over three successive stimulus cycles. Right column: Overlaid cycle histograms (bin width 1 ms) showing for trials 1–3 (top), 4–6 (middle), and 7–9 (bottom) the distribution of spike firing within the stimulus cycle during the initial and final 500 ms of the stimulus period.

the next higher value following each block of 5–10 stimuli (ISI 5 s). Only neurons having a well-defined skin region (''RF center'') that yielded a clear maximum in mean firing rate when exposed to 25 Hz flutter stimulation were studied in this way.

The pooled results from all 37 neurons are summarized in Fig. 9. Consistent with the published literature (e.g., Mountcastle *et al.*, 1969; see also Johnson, 1974), SI RA neuron responsivity (spikes/cycle) increased substantially and progressively as a function of stimulus amplitude (top left). Entrainment also increased progressively with increasing stimulus amplitude (middle panel on left)—this outcome is statistically highly significant (ANOVA, $p < 0.0001$). Phase angle of the response, on the other hand, decreased systematically with increasing amplitude of flutter stimulation (bottom panel on left), presumably reflecting the well-known more rapid onset of RA neuron spike firing with larger amplitude stimuli. The effect of amplitude on phase angle is statistically highly significant (ANOVA, $p < 0.0001$).

In order to test for temporal trends and their possible dependence upon stimulus amplitude, SI RA neuron responsivity, entrainment, and phase angle also were measured separately (for each of the 37 neurons) for the first vs last second of the spike train response evoked by each amplitude of 25 Hz stimulation. Figure 9 (right column) displays the 95% confidence intervals for the mean difference (last-second minus first-second values) in responsivity, entrainment, and phase angle as a function of stimulus amplitude. For each measure the overall mean last-second minus first-second difference is statistically highly significant: specifically, responsivity declined by 0.430 spikes/cycle ($p < 0.0001$), entrainment declined only slightly ($\Delta \mathbf{r}_b = -0.009$), but significantly ($p < 0.0001$), and phase angle increased ($\Delta\text{angle} = -30.84$ deg; $p < 0.0001$) between the initial and last (5th) seconds of stimulation. However, since the slope value of each relationship does not differ significantly from zero, the time-dependencies of responsivity, entrainment, and phase angle are unrelated to

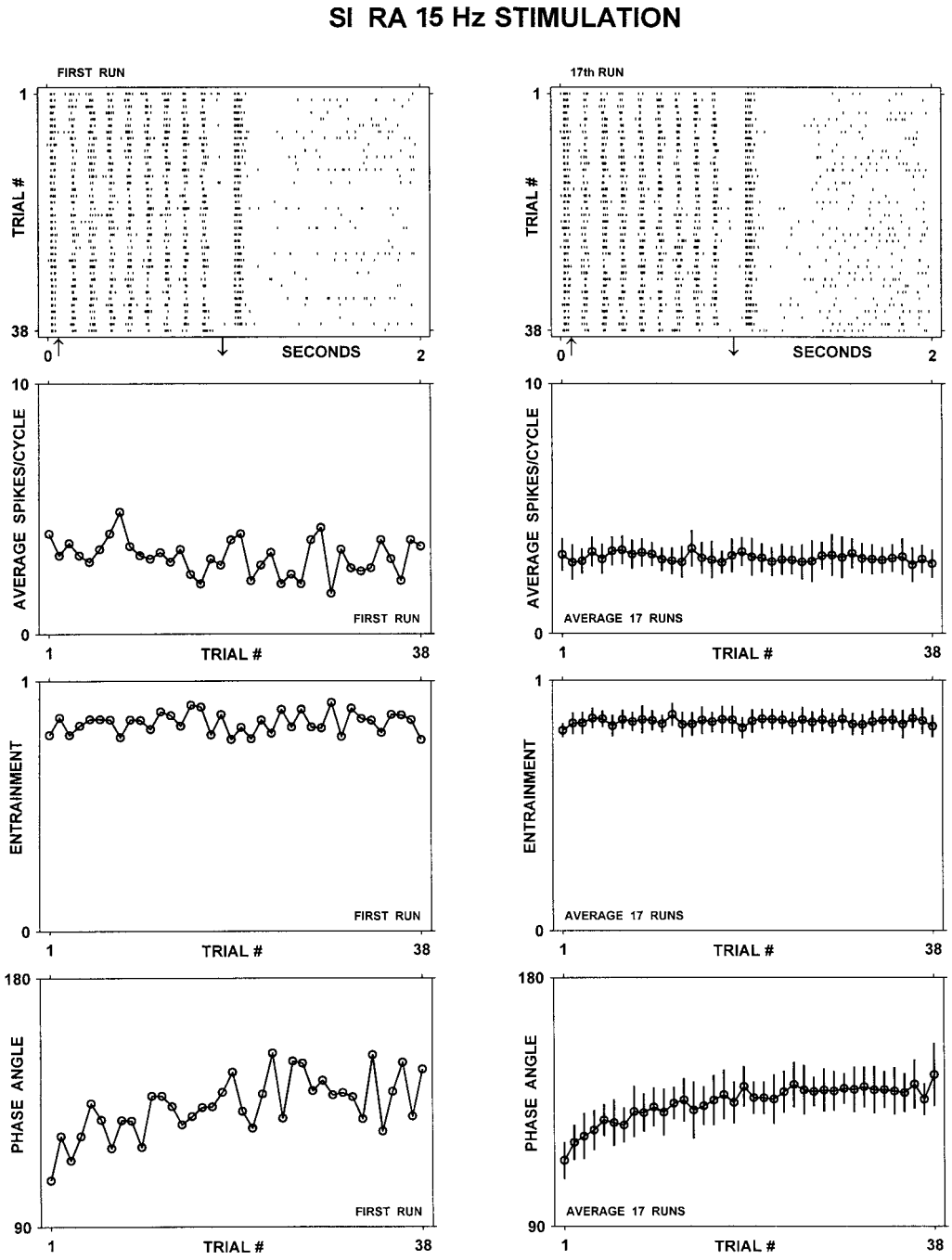

FIGURE 6. Reproducibility of SI RA neuron dynamics associated with rapid application of short-duration (0.8 s) 10 Hz flutter stimulation to the RF center (digit 3 pad; cat). Neuron in layer III of area 3b. Top panels: Raster plots showing neuron's spike discharge activity during first (left) and last run (17th; right). Stimulus conditions were the same in all runs: amplitude 100 μm peak-to-peak; 5 mm diameter contactor; ISI 1 s. A total of 36–38 stimulus trials were delivered in each run; time between successive runs varied between 3 and 15 min. Left column: Plots of responsivity vs trial number (2nd panel from top), entrainment vs trial number (3rd panel from top), and phase angle vs trial number (bottom), respectively—all constructed from the data recorded during the initial run. Right column: Plots of responsivity vs trial number (2nd from top), entrainment vs trial number (3rd from top), and phase angle vs trial number (bottom)—each point indicates the average for that trial over all 17 runs; brackets indicate ±1 SE.

stimulus amplitude (responsivity, $p = 0.628$; entrainment, $p = 0.082$; phase angle, $p = 0.675$).

The effect of *stimulus position relative to the RF center* on SI RA neuron responsivity and entrainment was investigated next. For the representative RA neuron illustrated in Fig. 10 delivery of the flutter stimulus to an off-center site in the RF not only evoked fewer spikes per stimulus cycle, but both entrainment and phase angle of the response modified substantially and differentially during stimulation. The qualitatively very different response dynamics associated with delivery of the same stimulus to a skin site outside the RF center are especially evident at the smaller stimulus amplitudes (25 and 50 μm)—compare on-center and off-center entrainment vs time, and phase angle vs time plots in Fig. 10.

Differential effects of on-center vs off-center flutter stimulation of the RF on SI RA neuron dynamics were especially prominent when long-duration

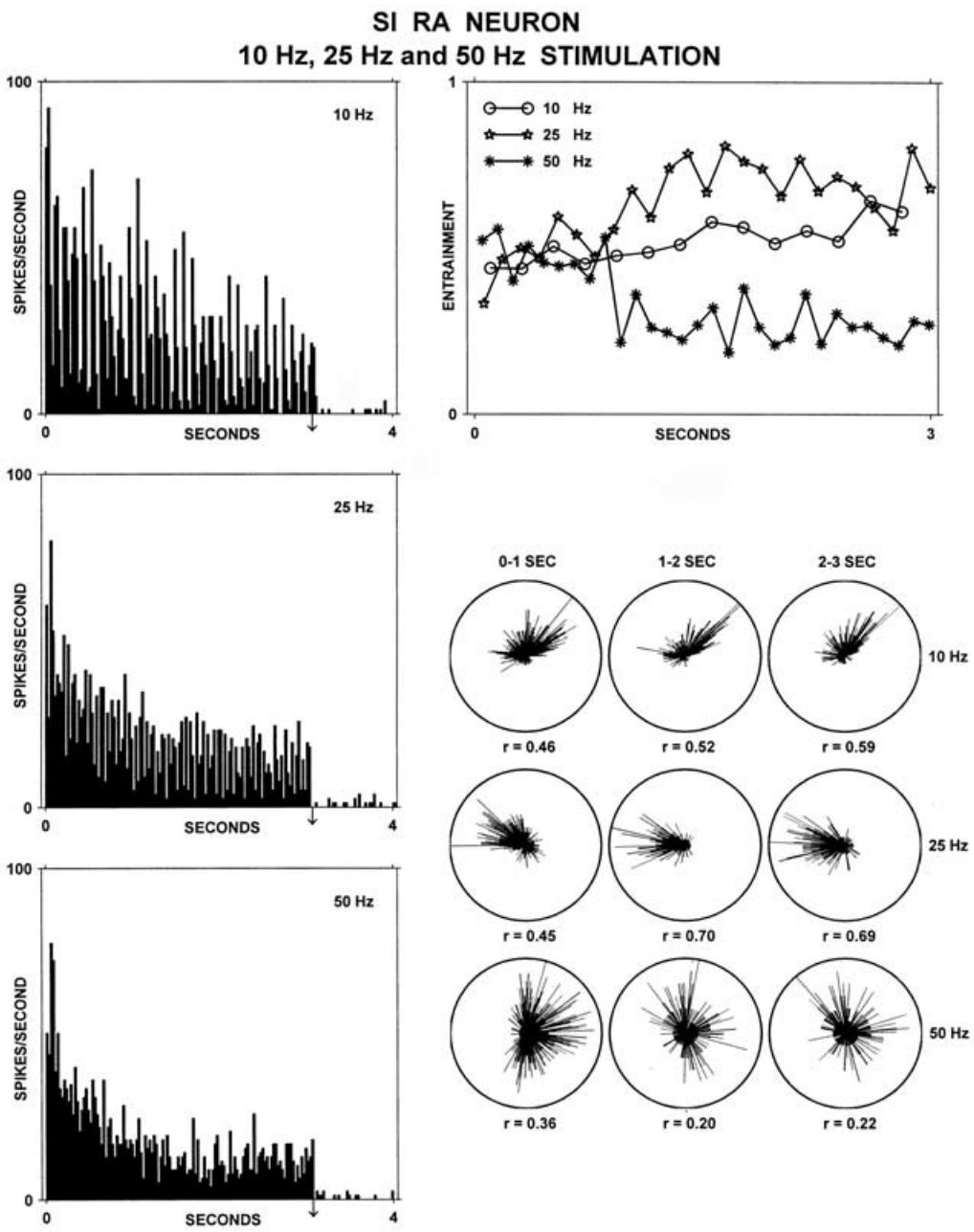

FIGURE 7. SI RA neuron response dynamics vary with frequency of stimulation. Layer IV neuron in area 1 (macaque monkey). Flutter stimuli of 10, 25, and 50 Hz were applied independently to RF center on middle phalangeal pad of digit 3; 5 mm diameter contactor; stimulus duration 3 s; peak-to-peak amplitude 250 μm; ISI 5 s. Left column: PSTs (bin width 25 ms). Panel at top right: Superimposed plots of entrainment vs time for the 10, 25, and 50 Hz stimuli. Each datapoint indicates the average over two (10 and 25 Hz stimulation), or over 5 successive stimulus cycles (50 Hz). Bottom right: Circular histograms computed for the activity recorded during three intervals (0–1 s, 1–2 s, and 2–3 s) after onset of each frequency of stimulation.

(15–30 s) flutter stimulation was used. For example, the responsivity of the neuron illustrated in Fig. 11 drops nearly to background levels by the end of a 15 s exposure to off-center flutter stimulation (PST; upper left panel). Also, the modest degree of entrainment present during the initial 1 s of stimulation virtually disappears (i.e., there is a prominent peak in the cycle histogram for spike discharge activity recorded in the initial 1 s of stimulation, but not in the cycle histogram for the activity during the last second of stimulation (14th–15th s; top right panel). Finally, the phase angle of the response follows an inverted U-shaped trajectory (early increase, later decrease) with increasing time after onset of stimulation (bottom left panel). These effects of ongoing flutter stimulation were reproducible: that is, essentially the same sequence of temporal changes in entrainment and phase angle occurred in both the first half (trials 1–14) and second half (trials 15–27) of the run—see pairs of entrainment vs time, and phase angle vs time plots in the column on the right of Fig. 11. In the study illustrated in Fig. 11 each 15 s stimulus period was separated from the next by an ISI of 30 s, to ensure that the trials were essentially independent.

While data such as those shown in Figs. 10 and 11 strongly suggest that stimulus position in the RF

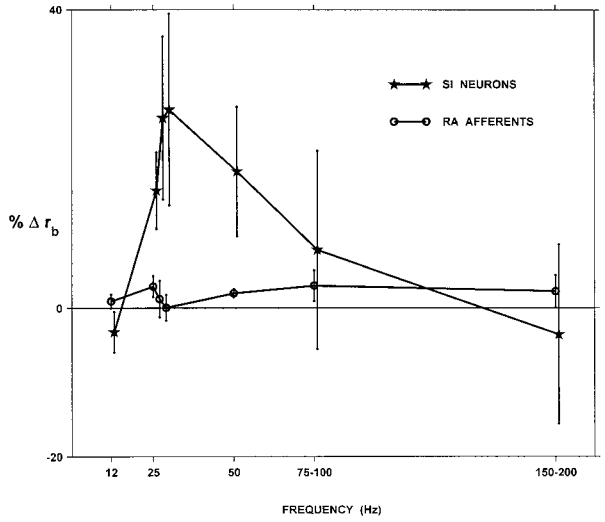

FIGURE 8. Effects of stimulus frequency on time-dependency of SI RA neuron and RA afferent entrainment. Summary of data from 39 RA neurons and 24 RA afferents. At least three frequencies of stimulation to the RF center were used to study each neuron/afferent. Stimulus duration 2–3 s; peak-to-peak amplitude 200–350 μm; 5 mm diameter contactor. % $\Delta \mathbf{r}_b$ = (difference between entrainment measured during initial and final second of stimulation/entrainment measured in initial second) $\times$ 100. Positive % $\Delta \mathbf{r}_b$ indicates increase, negative% $\Delta \mathbf{r}_b$ indicates decrease in entrainment. The mean values of % $\Delta \mathbf{r}_b$ for SI RA neurons at 25 and 28 Hz are significantly different from zero ($p = 0.004$ and 0.034, respectively), and those at 30 and 50 Hz approach significance ($p = 0.056$ and 0.062, respectively). For the RA afferents only the value of % $\Delta \mathbf{r}_b$ at 50 Hz ($p = 0.002$) is significantly different from zero. Brackets indicate ± 1 SE.

influences the form of the response dynamics exhibited by an SI RA neuron, we recognized that a related but by no means identical feature—position of the neuron within the responding SI neuron population—might influence SI RA neuron dynamics in a more consistent and orderly way. This was anticipated because of the large diversity in the size and location of the RFs of neurons which occupy the same cortical cell column (Favorov and Whitsel, 1988a,b); and also because the physical position of the RF "center" (the region that responds maximally to stimulation) in the RF can vary widely from one neuron to the next (Mountcastle, 1984; Favorov and Whitsel, 1988a,b). In our view the most elegant means presently available for evaluating this possibility consists of directly measuring the global SI population response to a stimulus using OIS imaging techniques, and subsequently using the same stimulus to characterize the spike train responses of RA neurons located in contrasting regions of the optical response pattern.

Fig. 12 shows results obtained from a combined OIS imaging/microelectrode recording experiment (see figure legend for additional details). The PST histograms (left) indicate that in this subject SI RA neuron responsivity (spikes/s) to the flutter stimulus that was delivered was high and well maintained over the entire stimulus period both at the site of maximal optical activity (the "OIS center"; "point 0") and at a site 250 μm away, while a very abrupt decline in responsivity occurred at distances 250–750 μm from the OIS center. Furthermore, the observations in Fig. 12 show that at 1,000 μm from the OIS center the RA neuron spike discharge activity recorded during stimulation was near-background; and at 1,250 μm it was possibly even below-background. Similarly (see entrainment vs time plots at upper right), RA neuron entrainment was high and declined modestly throughout the full period of stimulation at the OIS center, deteriorated with time at all sites outside the OIS center, and especially at the edge of the maximally activated SI region.

Sixty-five recordings of SI RA neuron spike discharge activity (from six squirrel monkeys studied in the same way; including the subject shown in Fig. 12) were divided into three groups based solely on the position of the recording site in the optical response pattern. Specifically, the first group ("CENTER"; $n = 27$) consists of recordings obtained within the centrally located zone in which the optical response was maximal—defined as the SI region occupied by pixels with absorbance values $\geq 95\%$ of the maximum; the second group ("BORDER"; $n = 23$) contains recordings carried out in an annulus of cortex located immediately adjacent to the maximally activated region, and occupied by pixels falling within the next 10–15% of the absorbance distribution; and the third group ("PERIPHERY"; $n = 15$) is comprised of recordings from the extensive zone that surrounds the outer margin of border cortex—defined as the region in which absorbance values were 20–80% of the maximum.

The regression lines in Fig. 13 summarize quantitatively the observed relationship between SI RA neuron entrainment and locus of the recording site within the SI global response pattern evoked by flutter (25–28 Hz) stimulation. Entrainment of the RA neuron activity recorded at each site was measured as a function of temporal position within the period of stimulus exposure, and the results combined within groups (as described in the preceding paragraph) and evaluated using linear regression analysis. Figure 13 shows that the regression lines computed for the three groups are completely disjoint (bounding dotted lines indicate 95% confidence intervals). For recordings of SI RA neuron activity carried out *within* the zone of maximal optical activity (obtained in the "central" zone) average entrainment was high, and tended to be relatively well maintained throughout the period of stimulation (the slope of the best fitting regression line is slightly negative, but not significantly different from 0). The entrainment performance of recordings in this group sometimes approached that of RA afferents in both absolute level and temporal stability. In contrast, for recordings carried out in the zone most remote to the region of maximal activation (in the "periphery") SI RA neuron entrainment tended to be far lower in absolute value, and it declined slightly, but significantly (slope $= -0.055$; $p < 0.001$) with increasing

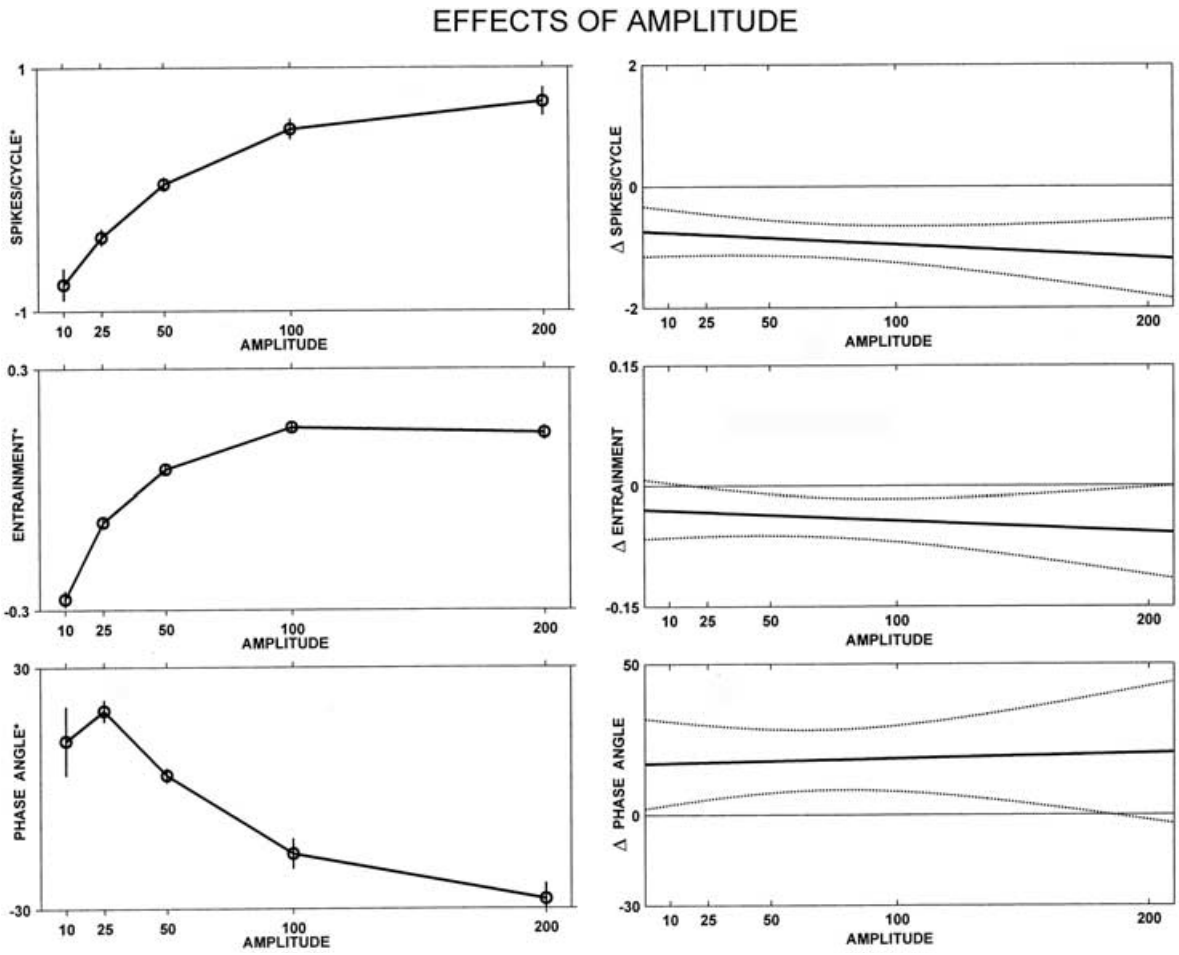

FIGURE 9. Effects of stimulus amplitude. Summary of data obtained from 37 SI RA neurons. All stimuli were 25 Hz, 5 s duration. Stimuli were applied to the RF center using a 5 mm diameter contactor. Five to ten trials at each amplitude. On left: Plots showing the amplitude-dependence of overall SI RA neuron responsivity (top), entrainment (middle), and phase angle (bottom). Values were normalized relative to largest value for each unit, to remove large between-unit differences in absolute magnitude. Brackets indicate ±1 SE. On right: Analysis showing that the changes observed to occur in RA neuron responsivity, entrainment, and phase angle between first and last second of stimulation are independent of stimulus amplitude. See text for details.

time after stimulus onset. The most interesting recordings, functionally speaking, are those obtained in penetrations performed in the "border" cortex where RA neuron entrainment tended to be moderately high at stimulus onset, but thereafter declined sharply and progressively (and statistically highly significantly; slope = −0.358; $p < 0.00001$) as stimulation continued.

To recapitulate, we so far have described reproducible SI RA neuron response dynamics, and shown how these dynamics are influenced by factors such as the frequency and amplitude of flutter stimulation, position of the stimulus in the RF, and recording location within the global SI response pattern. However, the implications of these unit-level observations for the ability of the responding SI RA neuron population as a whole to signal the attributes of skin flutter stimulation are not yet clear. For example, even if individual SI RA neurons do become progressively better entrained by an ongoing flutter stimulus, their collective response would not improve commensurately unless their periodic responses were also coordinated ("synchronized") so that they occurred at or near a common phase angle (i.e., so that the across-neuron periodic response was coherent). At the other extreme it also is conceivable that improved SI RA neuron synchrony could by itself lead to an improved population-level representation of stimulus frequency even if none of the participating neurons, individually, was improving its entrainment response. In order to understand the implications of the observed RA neuron response dynamics for the SI population-level response to flutter, therefore, we sought to assess if the response dynamics exhibited by different RA neurons in the responding region of SI in the same subject do, or do not, become more coherent with continuing stimulation.

Fig. 14 provides information that we suggest indicates across-neuron coordination, at an extremely local scale within SI, of the time-dependent changes in entrainment and phase angle exhibited by different RA neurons during the delivery of a skin flutter stimulus. This type of information was obtained at points during a microelectrode penetration when the electrode sampled action potentials clearly differing in amplitude, and thus presumably attributable to different, but closely spaced RA

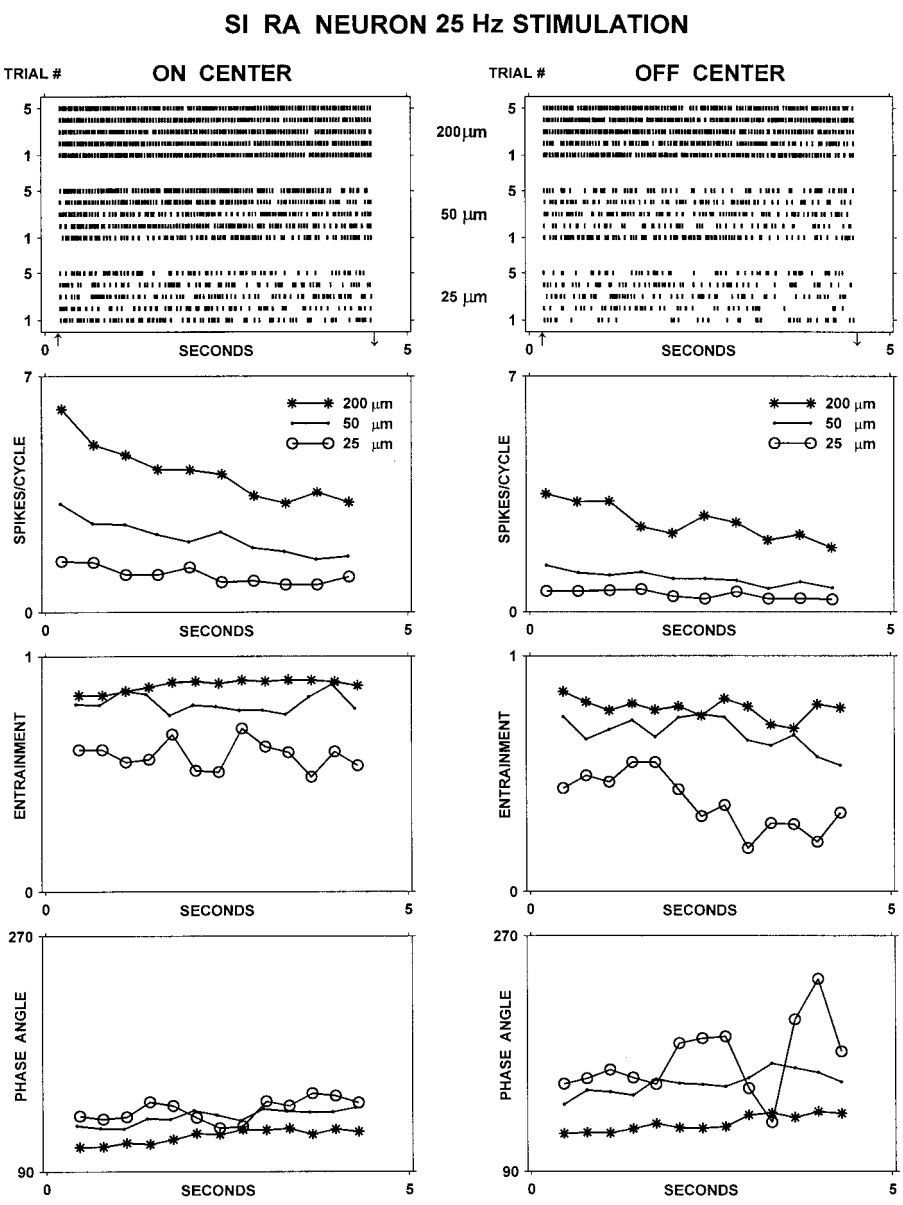

FIGURE 10. Effects of position in the RF on SI RA neuron response dynamics. Layer III neuron in area 3b (squirrel monkey). RF included most of the ulnar palmar skin on contralateral hand. Data shown in panels in left column ("on-center") were obtained using same stimulus conditions described in the legend to Fig. 9. Data in panels in right column ("off-center") were obtained in a subsequent run in which the same stimulus was delivered to a position 6 mm distal to the RF center. Panels at top: Raster plots showing spike train responses evoked from each skin site by five repetitions of each amplitude of stimulation (200, 50, and 25 µm peak-to-peak). Panels in 2nd, 3rd, and 4th rows from top: Plots of responsivity (spikes/cycle) vs time, entrainment vs time, and phase angle vs time for each stimulus amplitude. Each datapoint indicates the average over ten successive stimulus cycles.

neurons. In such instances non-overlapping voltage windows were used to discriminate action potentials on the basis of voltage, and each such "windowed" recording of RA neuron activity was independently analyzed to determine the temporal relationship between the flutter stimulus and the recorded spikes. The three rows of panels in Fig. 14 show the findings obtained from three such "window-discriminated" recordings obtained simultaneously from layer V in area 3b (squirrel monkey). Analysis revealed that entrainment and phase angle for each sample of RA neuron activity increased progressively (panels in 3rd and 4th columns from left). Furthermore, inspection of the cycle histograms generated for each recording (overlaid histograms in the left column) shows that with increasing time after onset of the flutter stimulus (1) the phase of the entrained response of each recording shifted progressively to a later point within the stimulus cycle—to a window between 19.7 and 22.9 ms (ratio plots in 2nd column from left), and (2) dispersion of spike activity within the stimulus cycle decreased significantly for each recording. Importantly, the ratio plots of Fig. 14 (2nd column from left) reveal that for each of the three recordings the temporal selectivity of the underlying dynamic process includes not only enhancement of spikes within a preferred time window located near to the end of the initial half-cycle of the stimulus period, but active suppression of spikes at either earlier or later times in the stimulus cycle. As a result, the degree of *synchrony* in the collective (across-neuron) pattern of spike discharge

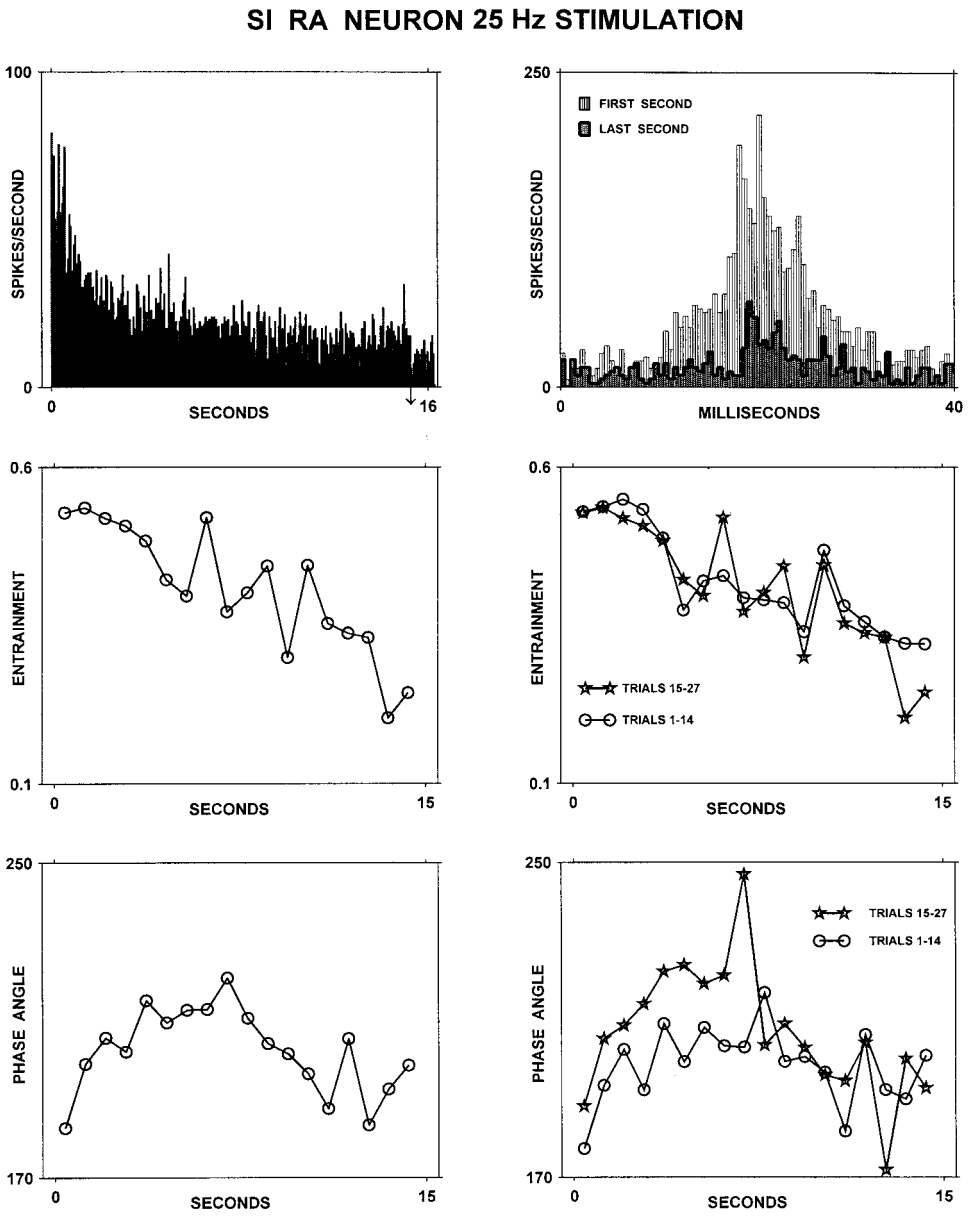

FIGURE 11. RA neuron dynamics associated with long-duration 25 Hz stimulation at an off-RF center locus. Area 1, layer V neuron located 300 μm posterior to the border between area 3b and area 1 (macaque monkey). RF included extensive portions of digits 2–5. The stimulus was applied to 5 mm proximal to RF center on the distal pad of digit 3. Peak-to-peak amplitude 350 μm; 15 s duration; ISI 30 s; 5 mm diameter contactor; 27 trials. Top panel on left: PST, 50 ms bin width. Top panel on right: Overlaid cycle histograms (bin width 0.5 ms) generated from activity recorded during 1st and 15th s of stimulus period. Panels on left: Entrainment vs time (middle), and phase angle vs time (bottom). Panels on right: Superimposed plots generated from the spike train data recorded during stimulus trials 1–14 and 15–27 (middle—entrainment vs time; bottom—phase angle vs time). Each datapoint indicates average over 33 stimulus cycles.

activity at this recording site (layer III in area 3b) improves with increasing time after stimulus onset. In summary, this local ensemble of three SI RA neurons undergoes similar changes in the phase angle of each spike train—the presumed functional significance of this neuron-to-neuron similarity in response dynamics is that this three-neuron spike firing pattern signals the periodicity of the evoking flutter stimulus more and more accurately with increasing time after stimulus onset (i.e., as stimulation continues this ensemble-level SI RA neuron spike firing pattern provides a progressively more coherent representation of the frequency of skin flutter stimulation).

Figure 15 displays the temporal trends in entrainment and phase angle detected in four simultaneous recordings of SI RA neuron spike discharge activity obtained from a different squirrel monkey. Once again, the recordings were obtained by voltage windowing the spike discharge activity recorded from a single microelectrode inserted into the SI region that responded maximally to cutaneous flutter stimulation. Note that all four recordings exhibit both a rapid decline in responsivity (upper left panel), and an equally rapid improvement in entrainment (upper right) within the 1sts after stimulus onset. For three of the four recordings the improvement in entrainment is maintained through-

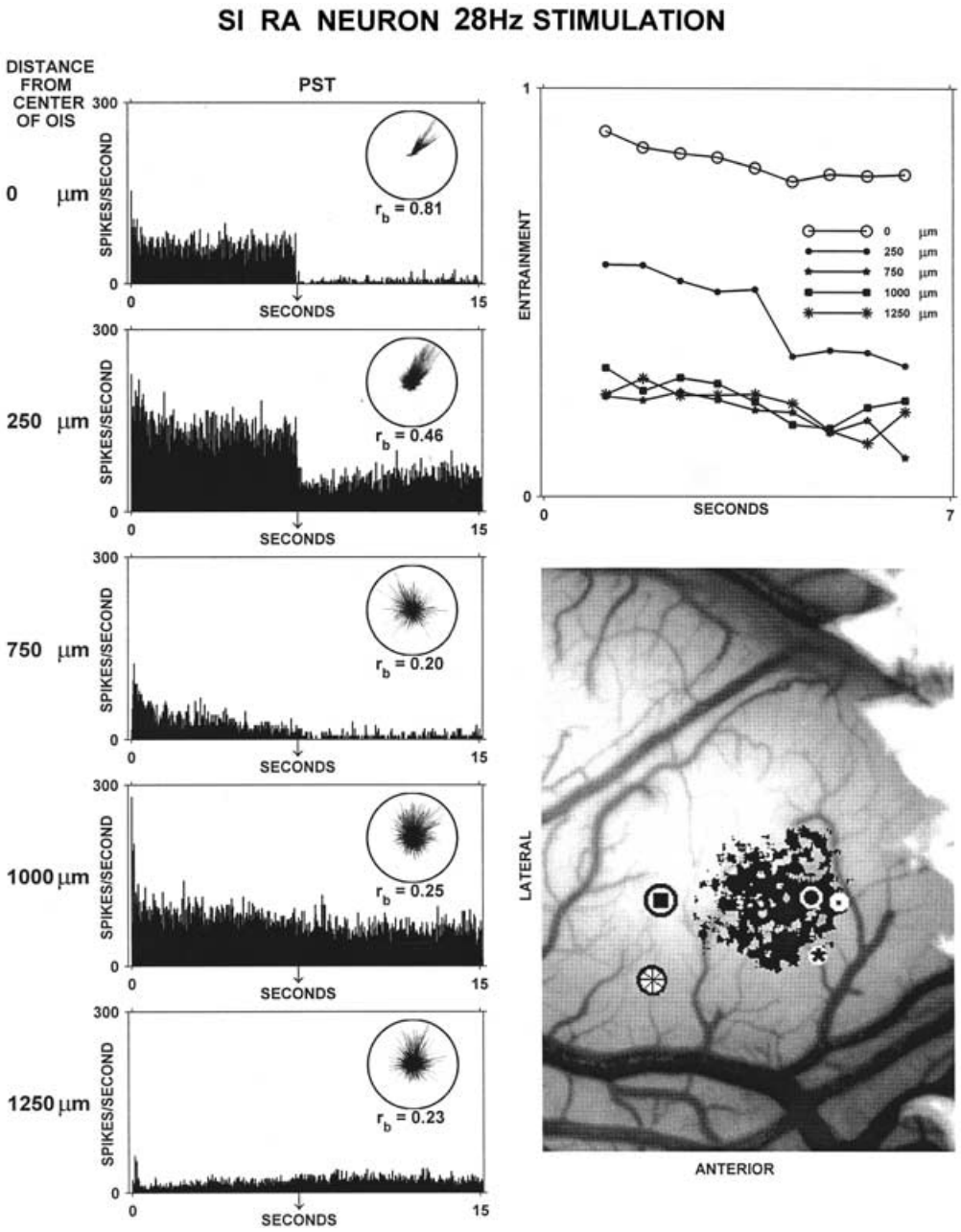

FIGURE 12. SI RA neuron dynamics at different locations within the responding region of SI. At each recording site the same flutter stimulus was delivered to the radial interdigital pad on the contralateral hand. Stimulus parameters were peak-to-peak amplitude 200 μm, duration 7 s, ISI 30 s. At each site 12–22 responses to this same stimulus were recorded. Left column: PST histograms showing the SI RA neuron mean firing rate response at different distances from the SI locus at which the OIS response evoked by the 28 Hz flutter stimulus was maximal. Circular histogram adjacent to each PST shows distribution of spike firing within the stimulus cycle at that recording site. Panel at top right: Plots showing time course of SI RA neuron entrainment at each of the five recording sites. Each datapoint indicates the average over 19 successive stimulus cycles. Bottom right: OIS image showing local region (black coding) in SI that underwent a near-maximal increase in absorbance (between 95 and 100% of the maximum) in response to the 28 Hz flutter stimulus. Labels (anterior, lateral) indicate image orientation.

out the period of stimulation, but for one (recording C) it is more transient. Another clear tendency (bottom left) is that the phase angles of the four responses differ widely at stimulus onset, and converge thereafter towards a common region of the stimulus cycle—in two of the four cases doing so from opposite directions (bottom right)! In sum, evidence like that presented in Figs. 14 and 15 is interpreted to indicate that the temporal trends in SI RA neuron responsivity, entrainment, and phase angle are *signs* of an across-neuron coordination (and thus an increased coherence of the ensemble-level RA neuron signal of the frequency of skin flutter stimulation) that occurs at least over distances spanning the cortical volume sampled by a single microelectrode—presumably a roughly spherical region of radius 50–200 μm (Mountcastle *et al.*, 1969). Further support for this interpretation is provided by our observations that in every set of simultaneous recordings of RA neuron spike discharge activity exam-

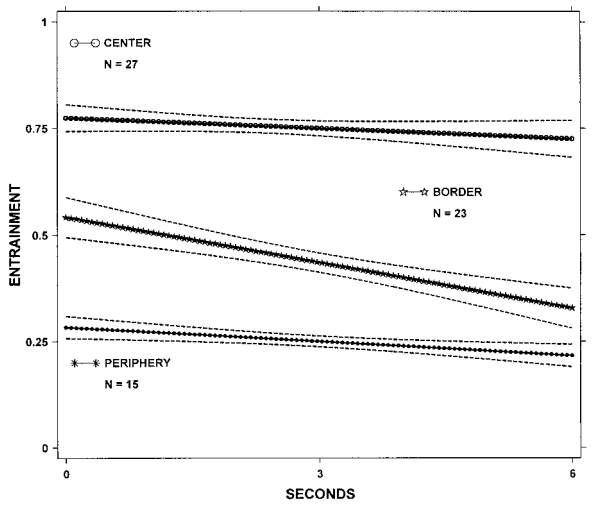

FIGURE 13. Effect of flutter stimulation on RA neuron entrainment depends on the position of the neuron within the responding population. Summary of data obtained in 65 recordings of SI RA neuron activity carried out in six subjects (squirrel monkeys). Position of each recording in global SI optical response pattern to flutter stimulation was ascertained by registration of OIS images with the locus of the microelectrode track. "CENTER", "BORDER", and "PERIPHERY" indicate SI regions defined by position within the flutter-evoked absorbance distribution (see text for details). As indicated in the text, each recording was assigned to one of three groups defined on the basis of the magnitude of the intrinsic signal at the position where the recording was obtained.

ined to date, on a trial-by-trial basis $\mathbf{r}_b$ for the data pooled over multiple windows was almost invariably higher than the trial-by-trial $\mathbf{r}_b$ for any of the individual windows, and it improved with increasing time after stimulus onset.

The observations illustrated in Figs. 16 and 17 move the inquiry to a larger spatial scale by showing the responses to the same flutter stimulus of multiple RA neurons recorded sequentially during individual microelectrode penetrations. Both of the penetrations shown in Fig. 16 were near-radial and thus, in the main, each sampled neurons occupying the same cortical column. In contrast, both of the penetrations shown in Fig. 17 possessed a large tangential component of movement, and therefore each penetration certainly encountered neurons in different columns. The radial penetrations in Fig. 16 generalize the results presented to this point, by suggesting that all aspects of the SI RA neuron response, including the large time-dependent changes in entrainment and/or phase angle that accompany RF center stimulation, are relatively consistent for neurons lying within the same column *regardless of their laminar location*. Figure 17, by contrast, indicates that a far greater diversity of temporal trends in entrainment and phase angle is characteristic of the

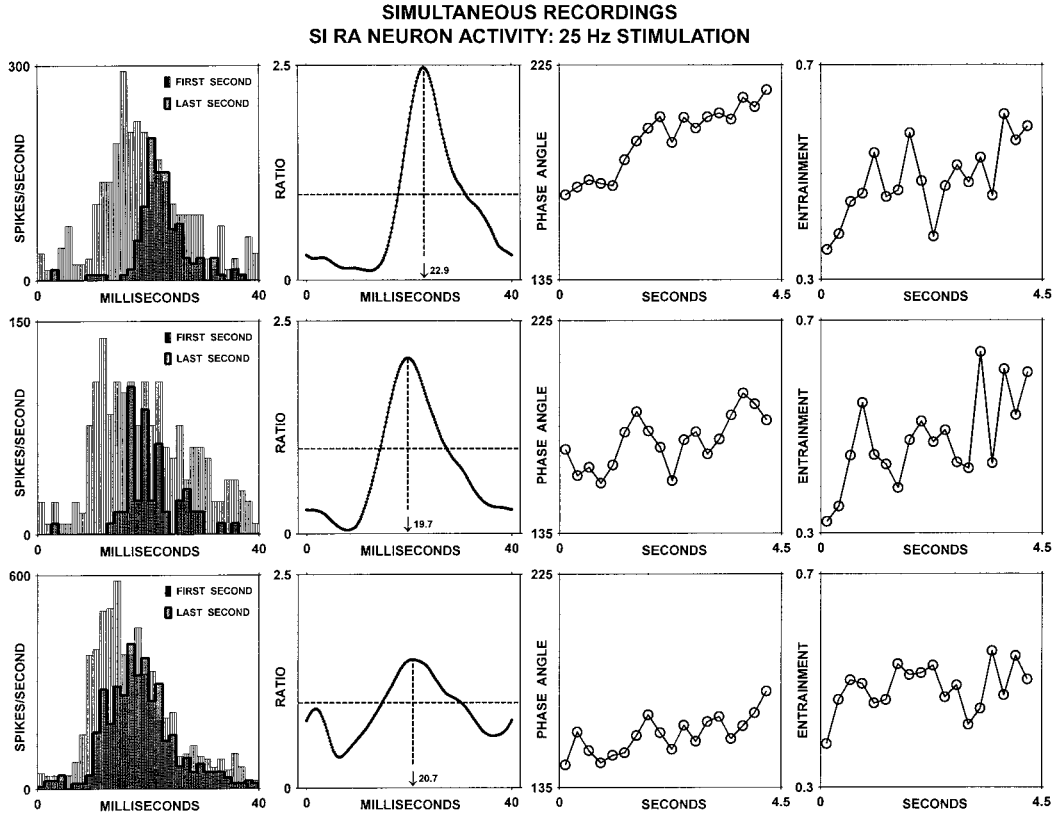

FIGURE 14. Data obtained from an SI site (layer V in area 1—squirrel monkey) where three recordings of stimulus-evoked SI RA neuron spike firing were obtained simultaneously—by voltage windowing the activity recorded by a single microelectrode. Top-to-bottom sequence of panels on left: Overlaid cycle histograms (bin width = 1 ms) showing distribution of spike activity in the stimulus cycle during first and last seconds of the stimulus period. Panels in 2nd column from left: "Ratio plots" (see Methods) showing, for each of the three recordings, the tendency for the magnitude of spike firing at a locus within the stimulus cycle to modify between first and last seconds of stimulation (ratio >1 indicates increased activity at locus in last second relative to the first; ratio < 1 indicates loss of activity at locus in last second relative to the first; ratio = 1.0 indicates no change, indicated in each ratio plot by dotted horizontal line). Panels in 3rd and 4th columns from left: Plot of phase angle vs time (3rd column) and entrainment vs time (4th column) for each recording. Each datapoint in plots in 3rd and 4th columns indicates average over six successive stimulus cycles.

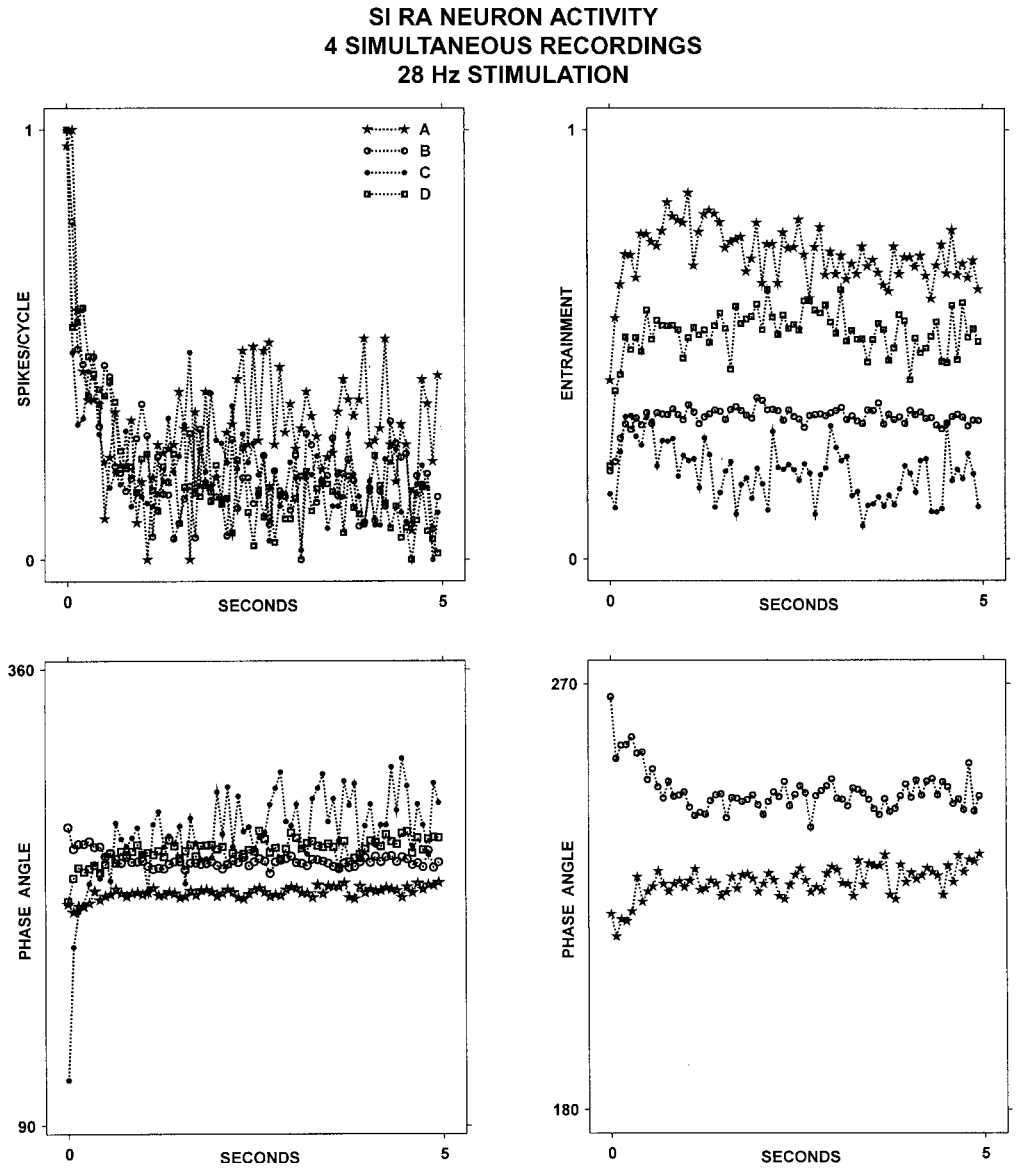

FIGURE 15. Results from four (A–D) simultaneous recordings of SI RA neuron spike firing. These recordings were obtained from a site in area 1 (layer III; squirrel monkey) using a single microelectrode. Stimulus parameters were frequency 28 Hz; peak-to-peak amplitude 250 μm; 7 s duration; ISI 10 s; 5 mm contactor. The stimulus was applied (20 trials) to the radial interdigital pad. Top plots: Responsivity vs time (on the left) and entrainment vs time (on the right) for each of the four recordings. Bottom plots: Plot of phase angle vs time (left) for each of the four recordings, and a replot of the phase angle vs time relationship for recordings A and B (right). Note that not only do the phase angles of responses A and B converge toward a common value during stimulation, but that they do so from opposite directions within the stimulus cycle (i.e., for recording A the phase angle of the response increases during stimulation, but for recording B the phase angle of the response decreases).

data obtained in microelectrode penetrations that sample RA neurons in different cell columns. We interpret findings such as those shown in Figs. 16 and 17 to indicate that the different forms of SI RA neuron response dynamics we have identified in our experiments are distributed, as predicted (Mountcastle, 1984), on a columnar basis within the responding region of SI cortex.

Discussion

The results of this study demonstrate that RA-type SI cortical neurons, unlike RA mechanoreceptive afferents studied using comparable stimulus conditions, frequently display systematic temporal trends in their response to a constant, suprathreshold flutter stimulus—not only in responsivity, but also in entrainment and the associated phase angle. Furthermore, the observations reveal that the form of these SI RA neuron response dynamics is influenced substantially and systematically by factors such as stimulus frequency, position of the stimulus within the RF, and especially position of the neuron within the global pattern of SI activation.

Previous studies have provided evidence of *population-level* response dynamics in SI cortex—these include not only OIS imaging studies (Tommerdahl *et al.*, 1999a,b), but also evoked potential recording and EEG studies. An extensive literature (for review see McLaughlin and Kelly, 1993), for example, demonstrates that SEP amplitude declines progressively as a function of

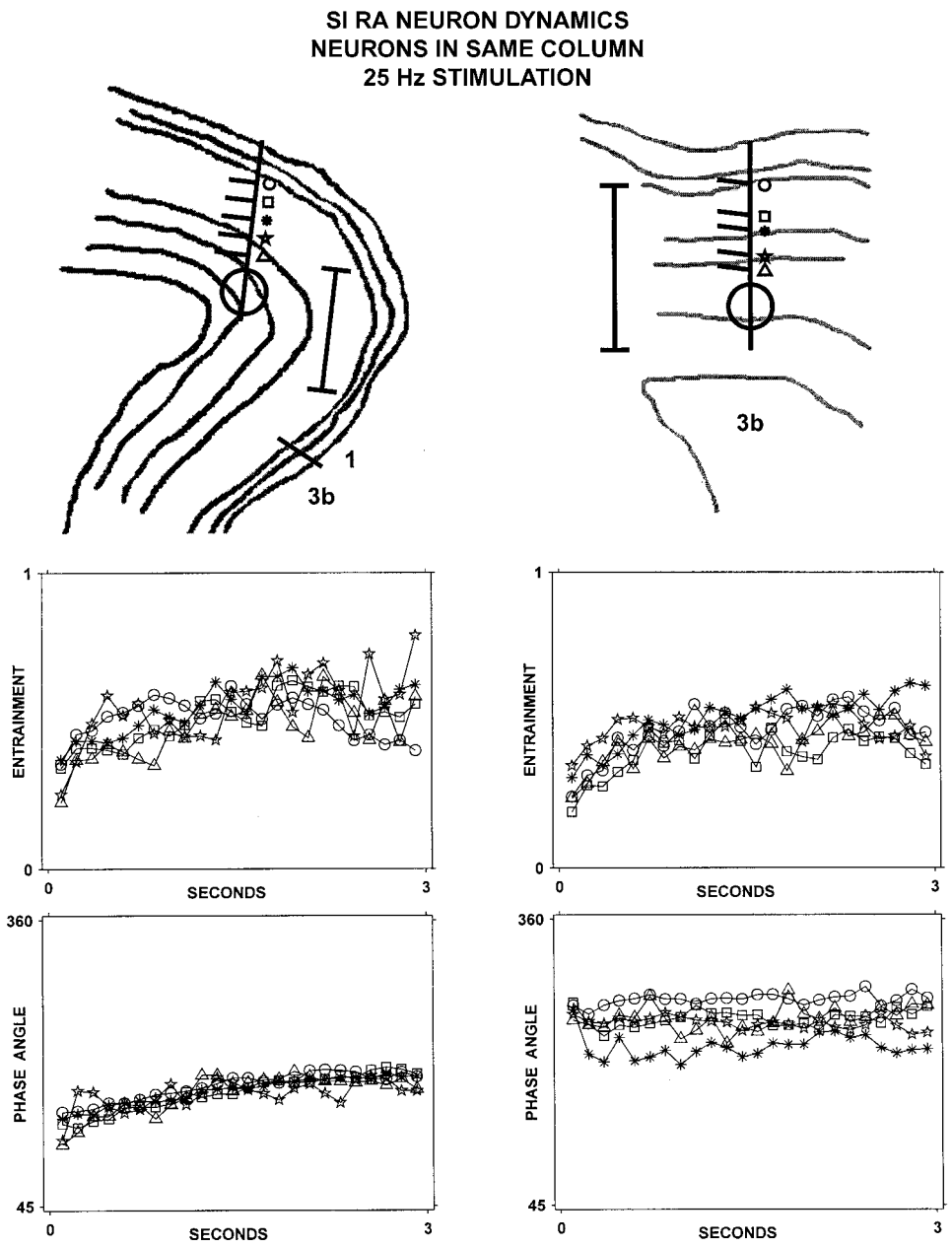

FIGURE 16. Consistency of the response dynamics exhibited by SI RA neurons in the same cortical column. Drawings at top: Intracortical trajectories of two near-radial penetrations—tics to left of each penetration indicate locations at which SI RA neuron activity was recorded. Scale bars = 1 mm. On the left: Five sites in area 1 at which RA neuron spike discharge activity was recorded during 25 Hz stimulation (3 s duration; peak-to-peak amplitude 350 μm; 5 mm diameter contactor; ISI 5 s) of the middle interphalangeal pad of digit 3 on the contralateral hand. On the right: Five sites in area 3b at which RA neuron activity was recorded during 25 Hz stimulation (3 s duration; peak-to-peak amplitude 400 μm; 2 mm diameter contractor; ISI 20 s) of the pad of digit 5 on the contralateral forepaw (cat). Panels at bottom: Superimposed plots of entrainment vs time (middle) and phase angle vs time (bottom) for the activity recorded at the five different sites in each subject. Each datapoint indicates average over three successive cycles.

decreasing time between stimulus presentations, especially for components of the SEP generated in the upper cortical layers. In addition, a high-resolution human EEG study by Kelly and Folger (1999) provided striking parallels to the finding (Tommerdahl *et al.*, 1999a,b) that in squirrel monkeys the global optical response of SI cortex to cutaneous flutter stimulation undergoes time-dependent funneling towards the region receiving its principal input from the stimulated skin locus. Kelly and Folger (1999) used frequency-domain analysis to detect periodic SI responses to skin flutter stimulation at the frequency of stimulation, and showed that these EEG "driving responses" underwent pronounced changes in amplitude and scalp topography during even brief (4 s) stimulus exposures. These temporal changes in the human SI response to constant flutter stimulation were both systematic and physiologically coherent, with the EEG driving response topography evolving toward that observed in the same subject during periodic microstimulation (using a percutaneous microelectrode) of a *single* mechanoreceptive afferent with a RF that occupied the same skin site stimulated with

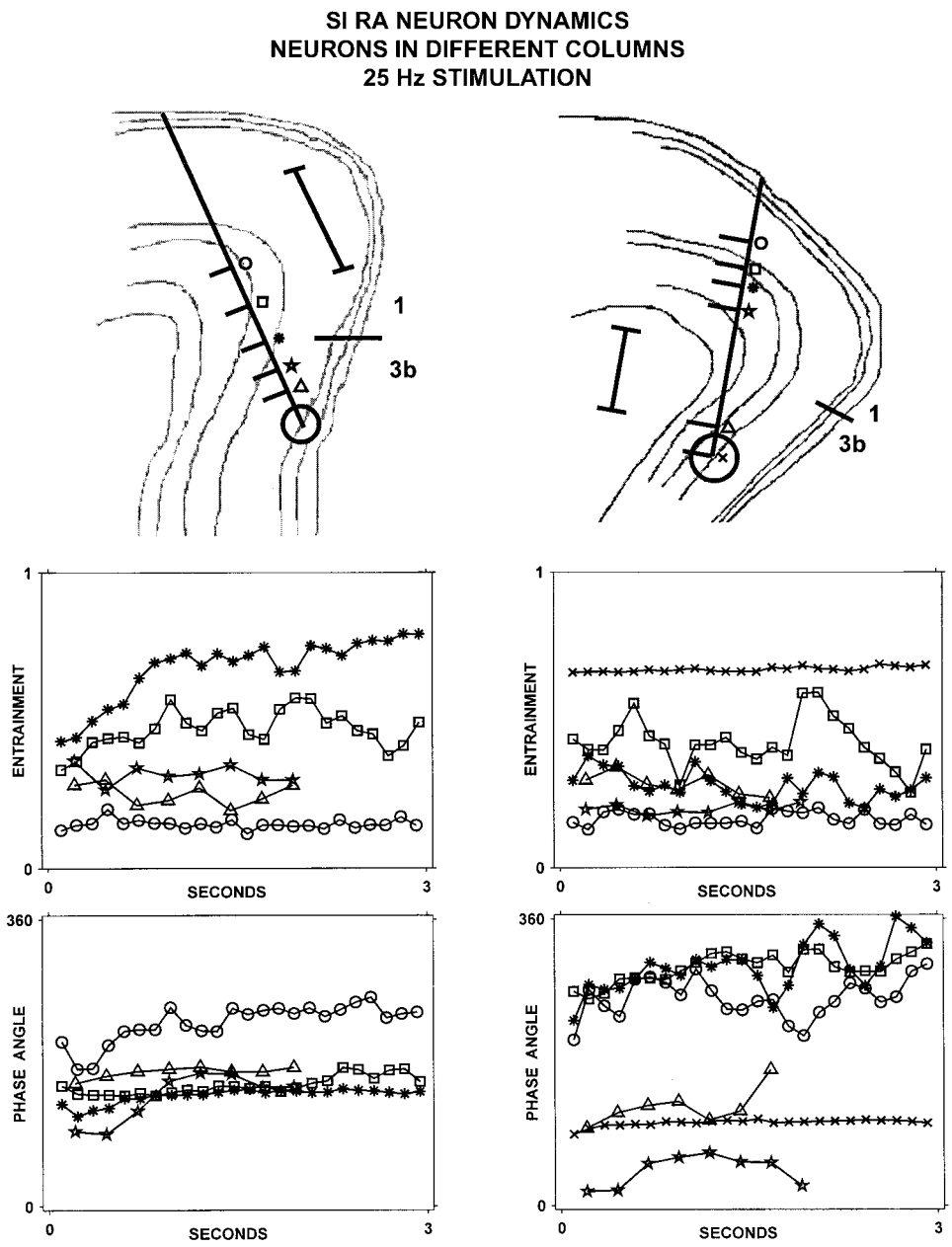

FIGURE 17. Diversity of response dynamics of SI RA neurons in different cortical columns. Format as in Fig. 15. Top left drawing: Five sites (located in layers III–V) at which RA neuron spike discharge activity was recorded during 25 Hz stimulation (duration 3 s; peak-to-peak amplitude 200 μm; 5 mm diameter contactor; ISI 2–5 s) of the distal pad of digit 3 of the contralateral hand (macaque monkey). Drawing at top right: Six sites (layers III–V) at which RA neuron activity was recorded during 25 Hz stimulation (duration 3 s; peak-to-peak amplitude 300 μm; ISI 5 s) of the distal pad of digit 2 of the contralateral hand (macaque monkey). Both penetrations sampled the activity of RA neurons in columns on opposite sides of the area 3b/1 boundary. Each datapoint in these entrainment vs time and phase angle vs time plots indicates average over three successive stimulus cycles.

the flutter stimulus (Kelly *et al.*, 1997; Trulsson *et al.*, 2001). Thus, much like the OIS evoked in SI of cat and squirrel monkey by flutter stimulation (Tommerdahl and Whitsel, 1996; Tommerdahl *et al.*, 1999a,b), the EEG driving response evoked in human SI cortex by a constant flutter stimulus is not static, but evolves temporally. This temporal evolution in the human SI response to flutter, moreover, was systematically accelerated by increasing the amplitude or frequency of the stimulus, and also by decreasing the interstimulus interval. In contrast, response dynamics were not detected in a population-level peripheral afferent response to flutter recorded in human subjects using electrodes on the skin at the level of the wrist (Kelly *et al.*, 1996).

The unit-level observations reported in the present study shed new light on the negative results reported by Mountcastle *et al.* (1969) regarding SI RA neuron response dynamics during skin flutter stimulation. That study emphasized the *fidelity* of the entrained SI RA neuron response to a small-amplitude (< 100 μm), brief (1 s) cutaneous flutter stimulus, delivered to the RF center at slow rates (1/5 s) with a small (2 mm diameter) contactor. Furthermore, the SI RA neurons studied by Mountcastle *et al.* (1969) mainly occupied the middle cortical layers which are subject to the strongest influences mediated by

direct, short-latency input from the skin. We regard the strong and stable SI RA entrainment responses described in the pioneering study of Mountcastle *et al.* (1969) as the limiting case or asymptote of the wider spectrum of RA neuron responses evoked by the diversity of mechanical skin stimuli encountered in everyday life. Interestingly, Mountcastle *et al.* (1969), p. 457) indicate that they did, in fact, observe declines in RA neuron responsivity during skin flutter stimulation (but "... only very rarely"), and that these tended to occur "... when the stimulus frequency is quite different from the 'best frequency' of a cortical neuron, or when the stimulus intensity is so high that appreciable repetitive firing occurs in each of the first few sine-wave cycles". The data analysis methods used by Mountcastle *et al.* (1969); cycle histogram analysis (with exclusion from the analysis of the part of the spike train record recorded within the initial 100–150 ms of stimulation) were not designed to detect or measure temporal dynamics in the entrainment of RA neuron spike discharge activity (or in the phase angle of the entrained response). In addition, the great majority of their results were obtained using near-threshold flutter stimulation of the RF. In contrast, in the present study we purposely *emphasized* the use of suprathreshold stimulus conditions because such stimuli are more representative of naturally occurring oscillatory mechanical skin stimuli, and utilized data analysis approaches recently demonstrated (Whitsel *et al.*, 2000, 2001) to possess the capacity to precisely quantify the responsivity, entrainment, and phase angle of the spike discharge response of RA neurons to very different stimulus conditions—including the responses to suprathreshold flutter stimuli. Our view is that when the very different stimulus conditions and data analysis procedures/strategies used in the different studies are considered, there is no fundamental conflict between the results of Mountcastle *et al.* (1969) and those reported here.

We turn now to the possible functional significance of the observed SI RA neuron response dynamics. Consider first, in general terms, the problem faced by SI cortex at the onset of a novel, *suprathreshold* skin flutter stimulus. The afferent drive evoked by a strong flutter stimulus to a digit tip, for example, sets up activity in an extremely large territory of SI—for example, the region of SI in macaque monkey that receives direct projections from the part of the ventrobasal thalamus that represents the skin of the tip of the index finger is estimated to be at least 20 mm^2 (Rausell *et al.*, 1992b; Jones, 2000). Moreover, a strong flutter stimulus engages broadly tuned neurons that respond, at least to some extent, to many different tactile stimuli. This early and widely distributed pattern of SI activation evoked by flutter stimulation presumably exhibits considerable spatial and temporal heterogeneities—because, for example, even on the local scale of a single SI segregate (a placed-defined SI cell column; Favorov and Whitsel, 1988a,b), single neuron RF sizes and shapes vary widely despite sharing a common skin point (the segregate RF center), and both SI neuron responsivity and latency of response depend strongly on the position of a stimulus within the cutaneous RF (Renkin, 1959; Diamond, 1989, p. 49). These characteristics make it apparent that a suprathreshold flutter stimulus will evoke periodic responses at many different locations within the SI global activation pattern and, at least initially, these responses will vary widely in strength, degree of entrainment, and phase of the entrained response. In addition, at moderate-to-large amplitudes of flutter stimulation the temporal pattern of the afferent drive that reaches RA neurons with RF centers close to the skin region directly contacted by the stimulator probe is likely to be of the $\mathbf{r}_2$ (bipolar) type (Talbot *et al.*, 1968, their Fig. 8; Johnson, 1974; Whitsel *et al.*, 2000; Kohn *et al.*, 2002). Given this initially widespread distribution of the SI activity evoked by a suprathreshold skin flutter stimulus, and given the anticipated considerable heterogeneity in RA neuron response magnitude, entrainment, and phase angle, how does the global SI response enable the relatively accurate estimation of stimulus locus, amplitude and frequency that has been demonstrated in numerous studies of human and animal vibrotactile sensibility?

Elsewhere we have introduced and progressively refined a model that we believe can account for many of the short-term SI RA neuron response dynamics reported in this paper (Whitsel *et al.*, 1989, 1991; Favorov and Kelly, 1994a,b, 1996a,b; Kohn *et al.* 2002). This model explicitly incorporates currently available information about cell types, their synaptic connectivity on micro- and macro-scales, receptor and neurotransmitter characteristics, and known aspects of SI topographical organization. The same model also has demonstrated through computer simulations its ability to reproduce a variety of experimentally established phenomena including the dynamic development of stimulus-evoked activation patterns (at both the macrocolumnar and minicolumnar level) which resemble the activation patterns detected in SI of living animals with both optical and metabolism-based (e.g., 2DG) imaging methods (Favorov and Kelly, 1994a,b; Favorov *et al.*, 2001).

The details of the above-described model are documented in the cited papers and will not be reproduced here. Its essence is a cascade of cellular/biophysical processes operating at a variety of time scales, which collectively enable the stimulus-evoked pattern of thalamocortical input drive to dynamically modify the effective functional connectivity within the responding region of the SI network. These modifications, mediated in part by the voltage-gated NMDA receptor system of the upper cortical layers, operate upon local differences in the initial SI global response pattern in such a way as to progressively

concentrate the response in those cells and cell columns best positioned to represent salient properties of the ongoing stimulus. We believe that the RA neuron response dynamics reported here, and the global functional neuroimaging results reported by Kelly and Folger (1999) and Tommerdahl *et al*. (1999a,b) provide glimpses, from varying perspectives, of these processes in action.

Our attempt in this paper to reconstruct the global SI response to suprathreshold flutter stimulation, though we believe it to be substantially correct, is necessarily limited by the narrow aperature through which we have so far been able to view the relevant phenomena—i.e., the aperture provided by recordings derived entirely from a few single neurons and small neuron groupings. A level of recording and analysis between single-unit activity and the scalp EEG (e.g., multichannel recording and analysis of unitary activity and/or local field potentials) would likely provide a wealth of new information not only about the dynamic evolution of the SI global response to cutaneous flutter, but associated properties such as dynamic changes in the coherence and phase relationships among the activities recorded at different SI sites (Singer, 1999; Varela *et al.*, 2001).

The SI RA neuron response dynamics detected in the present study appear to have functional implications closely parallel to recent findings reported in the rapidly burgeoning literature on short-term cortical plasticity (for review see Kohn and Whitsel, 2002). For both vision and audition, cortical-level dynamics have been observed that appear to be both pervasive and functionally significant, permitting the relevant region of sensory cortex to adjust its behavior adaptively, rapidly, and reversibly to currently prevailing stimulus conditions. In vision, for example, adaptation to an oscillating grating leads to reduced *absolute* perceptual sensitivity, but improved *differential* sensitivity to similar suprathreshold gratings presented subsequently. These effects, moreover, have been found in substantially parallel form at the single-unit, neural-population (EEG), and psychophysical levels of observation (e.g., Regan and Beverly, 1983; Regan and Beverly, 1985; Albrecht *et al.*, 1984; Ohzawa *et al.*, 1985; Bach *et al.*, 1988; Greenlee and Heitger, 1988; Bonds, 1991). Parallel results have been reported for human vibrotaction by Hollins and colleagues (Goble and Hollins, 1993, 1994; Hollins *et al.*, 1996), who showed that prolonged exposure (''adaptation'') to a flutter stimulus leads to improved discrimination of both the amplitude and frequency of brief suprathreshold test stimuli similar to the adaptor. It is believed that mechanisms in SI cortex account for frequency discrimination in the flutter range of stimulus frequencies, since this perceptual capacity is lost permanently following surgical destruction of postcentral cortex (LaMotte and Mountcastle, 1979).

The overall picture that emerges from the results presented in this paper is as follows: a prolonged or rapidly repeated flutter stimulus leads to a progressive concentration of the response in the region of SI which receives its principal direct input from the stimulated skin site. Within this region, and with increasing time after stimulus onset, the responses of individual RA neurons often tend to become both better entrained individually, and more synchronous collectively. Meanwhile, in neighboring regions of SI initially responsive to the stimulus, RA neuron responsivity and entrainment decline. It seems to us intuitively clear that such a process involving (1) improvement of the stronger and more reliable responses at the center of the cortical response pattern, and (2) suppression of the weaker and noisy responses in bordering cortex would support both improved differential SI responsivity to different frequencies of flutter stimulation delivered (at different times) to the same skin site, as well as improved SI signaling of the spatial locus of flutter stimulation. The finding by Vierck and Jones (1970) that the discrimination of two oscillating points delivered simultaneously to the skin improves progressively with continuing stimulation appears fully consistent with the operation of such a dynamic process. In addition, the finding that SI RA neuron entrainment but not RA afferent entrainment improves progressively with increasing stimulus amplitude (Fig. 9) appears consistent with the demonstration (Goff, 1967) that human frequency discrimination on the skin improves progressively with increasing amplitude of 40 Hz flutter stimulation.

While some of the time-dependent changes in SI RA neuron response develop continuously over periods of stimulation of 3–15 s or longer, others are expressed in periods of 100 ms or less, raising the question of whether such ultra-rapid SI dynamics could be functionally meaningful. This possibility is supported by findings obtained in recent studies of visual sensory cortex. Pack *et al.* (2001), for example, have shown that when individual neurons in the sensory cortical area MT (macaque monkey) are exposed to stimuli that provide conflicting information about the direction of local vs global motion, the neurons' initial response reflects local motion, but this response tendency is replaced within 100 ms or less by a progressively emerging representation of global motion direction. Perhaps more relevant is a study by Müller *et al.* (1999) which demonstrated that complex cells (but not simple cells) in macaque striate cortex adjust their orientation tuning to briefly presented sinusoidal gratings on a time scale corresponding to the durations typical of individual saccades. That these extremely rapid improvements in sensory cortical neuron discriminative capacity resulted from lateral interactions occurring within primary visual cortex was suggested by the fact that similar adaptation effects could be produced by

simultaneous presentation of a grating to the region surrounding the excitatory RF. Müller *et al.* (2001) have pointed out that various metabolic and information-transmission economies result from such effects, and suggested that large improvements in perceptual performance might, in general, result from relatively brief stimulus exposures. The data presented in this paper raise similar possibilities for somatosensation and, in particular, we wonder whether comparable ultra-short modifications of SI information processing and representation accompany the saltatory, repetitive movements characteristic of spontaneous haptic exploration—the ''haptic sniff''.

The findings of the present study also alerted us to the relevance of certain other published observations to SI neuron response dynamics. Of particular interest in this regard is the demonstration (Volgushev *et al.*, 1998; using subthreshold injected currents; rat V1 cortical slice; see also Lampl and Yarom, 1993) that sinusoidal 5–20 Hz modulation of layer II–III pyramidal neuron somal membrane potential exerts two remarkable effects: first, sinusoidal depolarization of the somal membrane selectively alters, via mechanisms intrinsic to the neuron, sensitivity to weak excitatory input so that such inputs lead to spike discharges *only* if they arrive during a narrow temporal window (a few ms) within the sinusoidal modulation cycle. Second, long-lasting NMDA receptor-mediated EPSPs generated by strong input generate spike discharges that, unlike the spikes evoked by the same input in the absence of sinusoidal depolarization of the soma, are precisely time-locked to the sinusoidal modulation cycle. If the findings of Vogelshev *et al.* (1998) apply to SI pyramidal neurons, both of the effects identified by their experiments could contribute powerfully to the dynamic synthesis of a synchronous population-level SI RA neuron driving response to flutter-evoked excitatory synaptic drive.

Our results also appear relevant to ongoing debates about synchronous oscillations in the excitability of CNS neurons and neuronal assemblies, their possible functional significance, and the underlying mechanisms (Ritz and Sejowski, 1997; Singer, 1999; Engel *et al.*, 2001; Jones, 2001; Varela *et al.*, 2001; Krahe *et al.*, 2002). First, the findings appear to blur the sharp distinction sometimes attempted between ''driven'' and ''induced'' CNS rhythms (Basar and Bullock, 1992). To us the term ''driven'' seems inappropriate when applied to primary sensory cortical pyramidal neurons, inasmuch as only a small fraction ($\sim$5%) of their synaptic input is thalamocortical, the remainder deriving from other cortical sources. More importantly, our results suggest that a prototypical ''driving'' stimulus, cutaneous flutter, engages the same intrinsic cortical pyramidal neuron mechanisms presumed by many to contribute to induced oscillations. Second, because the SI RA neuron response dynamics detected in this study (temporal increases in both the entrainment of single SI RA neurons and the synchrony of the responding SI RA neuron population) appear in principle able to explain the enhanced capacities to discriminate stimulus frequency and spatial locus (Vierck and Jones, 1970; Goble and Hollins, 1994) that develop during or shortly after a multisecond exposure to skin flutter stimulation, our results also support the recent proposals (Singer, 1999; Engel *et al.*, 2001) that the response of the CNS to ongoing sensory stimulation modifies dynamically and adaptively due to the intrinsic dynamics of spatially distributed cortical networks, and that across-neuron synchrony with precision in the millisecond range enhances the perceptual saliency of the CNS response to that stimulation.

Acknowledgements

The authors gratefully acknowledge the technical contribution of Calvin Wong. Dr K. A. Hester contributed to the early stages of the project as an NIDR Minority Investigator/Trainee supported by PO1DE07509, W. Maixner, Program Director. The experiments that addressed the effects of stimulus amplitude on SI RA neurons were a component of the doctoral dissertation research of Y. Li. The research was funded by NIH grants RO1NS34979, RO1NS37501, and a supplemental award to PO1DE07509 (B. L. Whitsel, P.I.).

References

ALBRECHT, D., S.B. FARRAR, and D.B. HAMILTON (1984) Spatial contrast adaptation characteristics of neurons recorded in the cat's visual cortex. *J Physiol (Lond)* **347:** 713–739.

BACH, M., M. GREENLEE, and B. BUHLER (1988) Contrast adaptation can increase visually evoked potential amplitude. *Clin Vision Sci* **3:** 357–372.

BASAR, E., and T.H. BULLOCK (1992) *Induced Rhythms in the Brain*, E. BASAR and T.H. BULLOCK, eds., Birkhauser, Boston.

BATSCHELET, A. (1981) *Circular Statistics in Biology*, Academic Press, London.

BONDS, A.B. (1991) Temporal dynamics of contrast gain in single cells of the cat striate cortex. *Vis Neurosci* **6:** 239–255.

BREDFELDT, C.E., and D.L. RINGACH (2002) Dynamics of spatial frequency tuning in macaque V1. *J Neurosci* **22:** 1976–1984.

BUONOMANO, D.V., and M.M. MERZENICH (1998) Cortical plasticity: from synapses to maps. *Ann Rev Neurosci* **21:** 149–186.

CELEBRINI, S., S. THORPE, Y. TROTTER, and M. IMBERT (1993) Dynamics of orientation coding in area V1 of the awake primate. *Vis Neurosci* **10:** 811–825.

CHUBBUCK, J.G. (1966) Small-motion biological stimulator, *APL Tech Digest* May–June: 18–23.

DAS, A., and C.D. GILBERT (1995) Receptive field expansion in adult visual cortex is linked to dynamic changes in the strength of cortical connections. *J Neurophysiol* **74:** 779–792.

DEANGELIS, G.C., I. OHZAWA, and R.D. FREEMAN (1995) Receptive-field dynamics in the central visual pathways. *TINS* **8:** 451–458.

DIAMOND, M.E. (1989) Organization of somatic sensory cortex: the detection of discrete topographic units and evidence for their integrative function. PhD dissertation, Department of Physiology, University of North Carolina at Chapel Hill.

DINSE, H.R., K. KRUGER, and J. BEST (1990) A temporal structure of cortical information processing. *Concepts Neurosci* **1:** 199–238.

ENGEL, A.K., P. FRIES, and W. SINGER (2001) Dynamic predictions: oscillations and synchrony in top-down processing. *Nat Rev Neurosci* **2:** 704–716.

FAVOROV, O.V., J.T. HESTER, D.G. KELLY, M. TOMMERDAHL, and B.L. WHITSEL (2001) Lateral interactions in cortical networks. In *Somatosensory Processing: From Single Neuron to Brain Imaging*, M.J. ROWE and Y. IWAMURA, eds. pp. 187–207, Harwood Academic, AustraliaChap. 12.

FAVOROV, O.V., and D.G. KELLY (1994a) Minicolumnar organization within somatosensory cortical segregates: I. Development of afferent connections. *Cereb Cortex* **4:** 408–427.

FAVOROV, O.V., and D.G. KELLY (1994b) Minicolumnar organization within somatosensory cortical segregates: II. Emergent functional properties. *Cereb Cortex* **4:** 428–442.

FAVOROV, O.V., and D.G. KELLY (1996a) Stimulus–response diversity in local neuronal populations in cerebral cortex. *Neuroreport* **7:** 2293–2301.

FAVOROV, O.V., and D.G. KELLY (1996b) Local receptive field diversity within cortical neuronal populations. In *Somesthesis and the Neurobiology of the Somatosensory Cortex*, O. FRANZEN, R. JOHANSSON, and L. TERENIUS, eds. pp. 395–408, Birkhauser Verlag, Basel, Switzerland.

FAVOROV, O.V., and B.L. WHITSEL (1988a) Spatial organization of the peripheral input to area 1 cell columns. I. The detection of ''segregates''. *Brain Res Rev* **13:** 25–42.

FAVOROV, O.V., and B.L. WHITSEL (1988b) Spatial organization of the peripheral input to area 1 cell columns. II. The forelimb representation achieved by a mosaic of segregates. *Brain Res Rev* **13:** 43–56.

FISHER, N.I. (1993) *Statistical Analysis of Circular Data*, Cambridge University Press, New York.

FRENCH, A.S., and A.V. HOLDEN (1971a) Alias-free sampling of neuronal spike trains. *Kybernetik* **8:** 165–171.

FRENCH, A.S., and A.V. HOLDEN (1971b) Semi-on-line implementation of an alias-free sampling system for neuronal signals. *Comput Programs Biomed* **2:** 1–7.

GHAZANFAR, A.A., and M.A.L. NICOLELIS (1999) Spatiotemporal properties of layer V neurons of the rat primary somatosensory cortex. *Cereb Cortex* **9:** 1047–3211.

GHAZANFAR, A.A., and M.A. NICOLELIS (2001) The structure and function of dynamic cortical and thalamic receptive fields. *Cereb Cortex* **11:** 183–193.

GHAZANFAR, A.A., C.R. STAMBAUGH, and M.A.L. NICOLELIS (2000) Encoding of tactile stimulus location by somatosensory thalamocortical ensembles. *J Neurosci* **20:** 3761–3775.

GOBLE, A., and M. HOLLINS (1993) Vibrotactile adaptation enhances amplitude discrimination. *J Acoust Soc Am* **93:** 418–424.

GOBLE, A., and M. HOLLINS (1994) Vibrotactile adaptation enhances frequency discrimination. *J Acoust Soc Am* **96:** 771–780.

GOFF, G.D. (1967) Differential discrimination of frequency of cutaneous mechanical vibration. *J Exp Psychol* **74:** 294–299.

GREENLEE, M., and F. HEITGER (1988) The functional role of contrast adaptation. *Vision Res* **28:** 791–798.

HASSLER, R., and K. MUHS-CLEMENT (1964) Architektonischer aufblau des sensorimotorischen und parietalen cortex der katze. *J Hirnforsch* **6:** 377–420.

HOLLINS, M., K.A. DELEMOS, and A.K. GOBLE (1996) Vibrotactile adaptation of the RA system: a psychophysical analysis. In *Somethesis and the Neurobiology of the Somatosensory Cortex*, O. FRANZÉN, R. JOHANSSON, and L. TERENIUS, eds. pp. 101–111, Birkhauser Verlag, Basel, Switzerland.

JOHANSSON, R.S., U. LANDSTROM, and R. LUNDSTROM (1982) Responses of mechanoreceptive afferent units in the glabrous skin of the human hand to sinusoidal skin displacements. *Brain Res* **244:** 17–25.

JOHNSON, K.O. (1974) Reconstruction of population response to a vibratory stimulus in quickly adapting mechanoreceptive afferent population innervating glabrous skin of the monkey. *J Neurophysiol* **37:** 48–72.

JONES, E.G. (2000) Cortical and subcortical contributions to activity-dependent plasticity in primate somatosensory cortex. *Ann Rev Neurosci* **23:** 1–37.

JONES, E.G. (2001) The thalamic matrix and thalamocortical synchrony. *TINS* **24:** 595–601.

JONES, E.G., and R. PORTER (1980) What is area 3a? *Brain Res Rev* **2:** 1–43.

KELLY, E.F., and S. FOLGER (1999) EEG evidence of stimulus-directed response dynamics in human somatosensory cortex. *Brain Res* **815:** 326–336.

KELLY, E.F., D.F. MCLAUGHLIN, W.J.R. DUNSEATH, S. FOLGER, and H.K. HUDNELL (1996) Frequency-domain measurement of vibrotactile driving responses in first-order afferent populations. *Exp Brain Res* **10:** 500–506.

KELLY, E.F., M. TRULSSON, and S.E. FOLGER (1997) Periodic microstimulation of single mechanoreceptive afferents produces frequency-following responses in human EEG. *J Neurophysiol* **77:** 137–144.

KOHN, A., C. METZ, M. TOMMERDAHL, and B.L. WHITSEL (2002) Stimulus-evoked modulation of sensorimotor pyramidal neuron EPSPs. *J Neurophysiol* **88:** 3331–3347.

KOHN, A., and B.L. WHITSEL (2002) Sensory cortical dynamics. *Behav. Brain Res* **135:** 119–126

KRAHE, R., G. KREIMAN, F. GABBIANI, C. KOCH, and W. METZNER (2002) Stimulus encoding and feature extraction by multiple sensory neurons. *J Neurosci* **22:** 2374–2382.

LAMOTTE, R.H., and V.B. MOUNTCASTLE (1979) Disorders in somesthesis following lesions of parietal lobe. *J Neurophysiol* **42:** 400–419.

LAMPL, I., and Y. YAROM (1993) Subthreshold oscillations of the membrane potential: a functional synchronizing and timing device. *J Neurophysiol* **70:** 2181–2186.

LEE, C.-J., and B.L. WHITSEL (1992) Mechanisms underlying somatosensory cortical dynamics. I. In vivo studies. *Cereb Cortex* **2:** 81–106.

LEE, C.-J., B.L. WHITSEL, and M. TOMMERDAHL (1992) Mechanisms underlying somatosensory cortical dynamics. II. In vitro studies. *Cereb Cortex* **2:** 107–133.

MALONEK, D., and A. GRINVALD (1996) Interactions between electrical activity and cortical microcirculation revealed by imaging spectroscopy: implications for functional brain mapping. *Science* **272:** 551–554.

MARPLE, S.L. JR (1987) *Digital Spectral Analysis with Applications*, Prentice-Hall, Englewood Cliffs, NJ.

MCKENNA, T.M., B.L. WHITSEL, D.A. DREYER, and C.B. METZ (1981) Organization of cat SI cortex: relations among cytoarchitecture, single neuron properties, and interhemispheric connectivity. *J Neurophysiol* **45:** 667–697.

MCLAUGHLIN, D.F., and E.F. KELLY (1993) SEPs as indices of adaptation in the somatosensory system. A review and prospectus. *Brain Res Rev* **18:** 151–206.

MERZENICH, M.M., R.J. NELSON, M.P. STRYKER, M.S. CYNADER, A. SCHOPPMAN, and J.M. ZOOK (1984) Somatosensory cortical map changes following digit amputation in adult monkeys. *J Comp Neurol* **224:** 591–605.

MOUNTCASTLE, V.B. (1984) Central nervous mechanisms in mechanoreceptive sensibility. In *Handbook of Physiology—The Nervous System*, Vol. 3, Chap. 18, pp. 789–878, Am. Physiol. Soc., Bethesda, MD.

MOUNTCASTLE, V.B., W.H. TALBOT, H. SAKATA, and J. HYVARINEN (1969) Cortical neuronal mechanisms in flutter vibration studied in unanesthetized monkeys. Neuronal periodicity and frequency discrimination. *J Neurophysiol* **32:** 452–484.

MULLER, J.R., A.B. METHA, J. KRAUSKOPF, and P. LENNIE (2001) Information conveyed by onset transients in responses of striate cortical neurons. *J Neurosci* **21:** 6978–6990.

OHZAWA, I., G. SCLAR, and R. FREEMAN (1985) Contrast gain control in the cat's visual system. *J Neurophysiol* **54:** 651–667.

PACK, C.C., V.K. BEREZOVSKII, and R.T. BORN (2001) Dynamic properties of neurons in cortical area MT in alert and anesthetized macaque monkeys. *Nature* **414:** 905–908.

PACK, C.C., and R.T. BORN (2001) Temporal dynamics of a neural solution to the aperture problem in visual area MT of macaque brain. *Nature* **409:** 1040–1042.

PETTET, M.W., and C.D. GILBERT (1992) Dynamic changes in receptive field size in cat primary visual cortex. *Proc Natl Acad Sci USA* **89:** 8366–8370.

POWELL, T.P.S., and V.B. MOUNTCASTLE (1959) Some aspects of the functional organization of the postcentral gyrus of the monkey: a correlation of findings obtained in a single unit analysis with cytoarchitecture. *Bull Johns Hopkins Hosp* **105:** 133–162.

RAUSELL, E., L. BICKFORD, P.R. MANGER, and E.G. JONES (1992) Extensive divergence and convergence in the thalamocortical projection to monkey somatosensory cortex. *J Neurosci* **18:** 4216–4232.

RECANZONE, G.H., M.M. MERZENICH, W.M. JENKINS, K.A. GRAJSKI, and H.R. DINSE (1992a) Topographic reorganization of the hand representation in cortical area 3b of owl monkeys trained in a frequency-discrimination task. *J Neurophysiol* **67:** 1031–1056.

RECANZONE, G.H., M.M. MERZENICH, and C.E. SCHREINER (1992b) Changes in the distributed temporal response properties of SI cortical neurons reflect improvements in performance on a temporally based tactile discrimination task. *J Neurophysiol* **67:** 1071–1091.

REGAN, D., and K.I. BEVERLY (1983) Spatial frequency discrimination and detection: comparison of post-adaptation thresholds. *J Opt Soc Am* **73:** 1684–1690.

REGAN, D., and K.I. BEVERLY (1985) Postadaptation orientation discrimination. *J Opt Soc Am* **112:** 147–155.

RENKIN, B.Z. (1959) Response of cortical neurons in the somatic sensory area I of the cat in relation to position and frequency of electrical stimulation within cutaneous receptive fields. Doctoral dissertation, The Johns Hopkins University.

RINGACH, D.L., M.J. HAWKEN, and R. SHAPLEY (1997) Dynamics of orientation tuning in macaque primary visual cortex. *Nature* **387:** 281–284.

RITZ, R., and T. SEJNOWSKI (1997) Synchronous oscillatory activity in sensory systems: new vistas on mechanisms. *Curr Opin Neurobiol* **7:** 536–546.

SHEVELEV, I.A., U.T. EYSEL, N.A. LAZAREVA, and G.A. SHARAEV (1998) The contribution of intracortical inhibition to dynamics of orientation tuning in cat striate cortex neurons. *Neuroscience* **84:** 11–23.

SHEVELEV, I.A., M.A. VOLGUSHEV, and G.A. SHAREV (1992) Dynamics of response of V1 neurons evoked by stimulation of different zones of receptive field. *Neuroscience* **51:** 445–450.

SHOHAM, D., and A. GRINVALD (2001) The cortical representation of the hand in macaque and human area S-I: high resolution optical imaging. *J Neurosci* **21:** 6820–6835.

SHTOYERMAN, E., A. ARIELI, H. SLOVIN, I. VANZETTA, and A. GRINVALD (2000) Long-term optical imaging and spectroscopy reveal mechanisms underling the intrinsic signal and stability of cortical maps in V1 of behaving monkeys. *J Neurosci* **20:** 8111–8121.

SINGER, W. (1999) Neuronal synchrony: a versatile code for the definition of relations? *Neuron* **24:** 49–65.

SUGASE, Y., S. YAMANE, S. UENO, and K. KAWANO (1999) Gobal and fine information coded by single neurons in the temporal visual cortex. *Nature* **400:** 869–873.

SUR, M., R.J. NELSON, and J.H. KAAS (1982) Representations of the body surface in cortical areas 3b and 1 of squirrel monkeys: comparisons with other primates. *J Comp Neurol* **211:** 177–192.

TALBOT, W.H., I. DARIAN-SMITH, H.H. KORNHUBER, and V.B. MOUNTCASTLE (1968) The sense of flutter-vibration: comparison of the human capacity with response patterns of mechanoreceptive afferents from the monkey hand. *J Neurophysiol* **31:** 301–334.

TOMMERDAHL, M., K.A. DELEMOS, B.L. WHITSEL, O.V. FAVOROV, and C.B. METZ (1999a) Response of anterior parietal cortex to cutaneous flutter *versus* vibration. *J Neurophysiol* **82:** 16–33.

TOMMERDAHL, M., and B.L. WHITSEL (1996) Optical imaging of intrinsic signals in somatosensory cortex. In *Somesthesis and the Neurobiology of the Somatosensory Cortex*, O. FRANZEN, R. JOHANSSON, and L. TERENIUS, eds. pp. 369–384, Birkhauser Verlag, Basel, Switzerland.

TOMMERDAHL, M., B.L. WHITSEL, O.V. FAVOROV, C.B. METZ, and B. O'QUINN (1999b) Responses of contralateral SI and SII in cat to same-site cutaneous flutter versus vibration. *J Neurophysiol* **82:** 1982–1992.

TRULSSON, M., S.T. FRANCIS, E.F. KELLY, G. WESTLING, R. BOWTELL, and F. MCGLONE (2001) Cortical responses to single mechanoreceptive afferent microstimulation revealed with fMRI. *Neuroimage* **13:** 613–622.

VALLBO, A.B., K.A. OLSSON, K.-G. WESTBERG, and F.J. CLARK (1984) Microstimulation of single tactile afferents from the human hand. *Brain* **107:** 727–749.

VARELA, F., J.-P. LACHAUX, E. RODRIGUEZ, and J. MARTINERIE (2001) The brainweb: phase synchronization and large-scale integration. *Nat Rev Neurosci* **2:** 229–239.

VIERCK, C.J., Jr. and M.B. JONES (1970) Influences of low and high frequency oscillation upon spatio-tactile resolution. *Physiol Behav* **5:** 1431–1435.

VOLGUSHEV, M., M. CHISTIAKOVA, and W. SINGER (1998) Modification of discharge patterns of neocortical neurons by induced oscillations of the membrane potential. *Neuroscience* **83:** 15–25.

WHITSEL, B.L., O. FAVOROV, K.A. DELEMOS, C.-J. LEE, M. TOMMERDAHL, G.K. ESSICK, and B. NAHKLE (1999) SI neuron response variability is stimulus-tuned and NMDA receptor dependent. *J Neurophysiol* **81:** 2988–3006.

WHITSEL, B.L., O.V. FAVOROV, D.G. KELLY, and M. TOMMERDAHL (1991) Mechanisms of dynamic peri- and intracolumnar interactions in somatosensory cortex: stimulus-specific contrast enhancement by NMDA receptor activation. In *Information Processing in the Somatosensory System*, O. FRANZEN and J. WESTMAN, eds. pp. 353–369, Macmillan, London.

WHITSEL, B.L., E.F. KELLY, K.A. DELEMOS, M. XU, and P.M. QUIBRERA (2000) Stability of RA afferent entrainment *vs.* responsivity. *Somatosens Mot Res* **17:** 13–31.

WHITSEL, B.L., E.F. KELLY, M. XU, M. TOMMERDAHL, and P.M. QUIBRERA (2001) Frequency-dependent response of SI RA-class neurons to vibrotactile stimulation of the receptive field. *Somatosens Mot Res* **18:** 263–285.